6-1-2009

Investigation of atmospheric microplasma jet for nanofabrication

Konstantin Yurchenko

Investigation of Atmospheric Microplasma Jet for Nanofabrication

By
Konstantin J. Yurchenko

A Thesis Submitted in
Partial Fulfilment
of the Requirements for the Degree of

MASTER OF SCIENCE
In
Material Science and Engineering

Approved by:

Thesis Advisor:_____
Dr. Davide Mariotti

Committee Member:_____
Dr. Lynn Fuller

Committee Member:_____
Dr. Kalathur Santhanam

Center for Material Science and Engineering
Rochester Institute of Technology
Rochester, New York
June, 2009

Investigation of Atmospheric Microplasma Jet for Nanofabrication

I, Konstantin J. Yurchenko, hereby grant the permission to the Wallace Library of the Rochester Institute of Technology to reproduce my thesis in whole of in part. Any reproduction will not be for commercial profit.

Date:_____ Author:_____

Acknowledgments

The work done on this thesis over the past year would have not been possible without the help of several people in and outside of RIT. I would like to thank my advisor and mentor Dr. Davide Mariotti most of all for the direction and support he has provided along the way. He has given me valuable insight and an intuitive view on the behaviour of atmospheric microplasma, as well provided me with knowledge and tools required to understand the physics behind it.

I would also like to thank my committee members, Dr. K.S.V. Santhanam and Dr. Lynn Fuller, for their help in carefully reviewing the thesis and providing feedback. The SMFL staff, particularly Scott Blondel, John Nash, and Bruce Tolleson, who has given much of their time and patience in helping me to overcome challenges I was facing during the design of the system.

Investigation of Atmospheric Microplasma Jet for Nanofabrication

By

Konstantin J. Yurchenko

Masters of Science in Material Science and Engineering

Abstract

The last decade has seen an immense amount of research exploring advanced nanofabrication techniques. Many efforts on this front have moved closer to realization of industrially viable nanofabrication, i.e. nanomanufacturing.

Plasma-assisted processes have proven to be particularly suitable for nanofabrication due to a non-equilibrium condition that offers high concentration of chemically reactive species at low gas temperatures. Recently, cost-effective atmospheric plasma technologies have been a subject of intense research. The possibility of producing plasma environments at atmospheric pressure similar to those found at low-pressure offer additional advantages for industrial implementation of nanofabrication processes and surface treatment. Atmospheric pressure equates to lower processing cost, higher reaction rates, and increased throughput. An effective way to produce plasmas at atmospheric pressure while maintaining a high degree of process flexibility is to confine them in sub-millimeter cavities, i.e. microplasmas.

In this contribution, we have developed atmospheric microplasma systems and their applicability to nanofabrication is being considered. Contemporary research reports that plasma properties in the sub-millimeter range possess peculiar characteristics and a unique chemistry. The experiments described in this thesis aim to investigate these qualities. Discharge properties are examined using current-voltage measurements, optical emission spectroscopy, temperature measurements and optical photography and compared to numerical analysis. Preliminary results on the application of this plasma system to nanofabrication and surface treatment are provided.

Table of Contents

Table of Figures

1. Atmospheric microplasma processing

1.1. Stated purpose of the study

The scope of this work is focused on the development of a system capable to produce non-thermal gas discharges in an atmospheric environment. The design of the planned system allows generating plasma that operates in a microplasma regime. Such plasmas do not require vacuum and increase process cost efficiency, as expensive auxiliary pumping equipment is not required. Due to this advantage, applications of atmospheric microplasmas can pave a way to an increase in throughput. A system like the one described here offers some unique properties that are useful for advanced material processing and biomedical applications [1].

Atmospheric plasmas in general are employed for processing substrates of complex geometry and pressure sensitive materials can be handled without additional damage. Atmospheric microplasma regime offers chemical environments that incorporate this feature and also lead to production of new materials. Atmospheric microplasmas are of great interest due to their practicability in producing nanocrystaline materials. To explore this possibility, synthesis of carbon-based materials and deposition of nanostructured metal oxides is attempted with the developed system and obtained results are reported here.

In general, plasma is extremely ubiquitous in manufacturing industry. It is used for treatment of polymers, paper, wood, fabric, and silicon. Recently, modification of tissue, cells and proteins using plasmas has been explored. Plasmas require less energy comparing to that consumed by the traditional ways of sterilization of biologically

contaminated materials and that is why plasma processing technologies can be key to practical and sustainable manufacturing in the modern world. [2]

1.2. Brief overview of plasma theory

A conglomeration of atoms on a large scale makes up all matter. Depending on the way, atoms interact a general distinction between the states of matter can be made. Plasma state is produced when electrons are stripped from gas atoms through an addition of energy. This physical process is known as ionization. Ionization process can be accomplished through supplying the gas with either thermal or electrical energy. In some other instances, ultraviolet or intense visible light can also play role as an example. The approximate ionization potentials for helium and argon are 24.5 eV and 16 eV respectively [3]. These gases are commonly used for basic plasma study.

When the added energy is sufficient for electrons to overcome an electric potential barrier that confines them to the molecules or atoms of the gas, chemically reactive ions are also formed. These together with the electrons, neutral atoms and molecules constitute the bulk of the plasma. Collisions among them can lead to further reactions such as chemical dissociation. Furthermore, photons are emitted as the species become de-excited during the plasma's lifetime. On the large scale, plasma is a balanced interaction of these species. However, freely moving electrons play a major and a fundamental role in plasma. They enhance further ionization and can be accelerated by electro-magnetic fields. The kinetic energy of the electrons can be affected either through an elastic or inelastic collision with an ion or interaction with an electric field.

Since, ions and electrons move at a particular average velocity, an average kinetic energy for either can be determined. This defines a distinction in the temperatures that

may develop within the plasma. Having two types of temperature within the plasma, that of ions and electrons, gives rise to two categories in which plasmas can be generalized. In the first category, the temperatures of electrons and ions are comparable. Such plasmas are called thermal. The constituents (ions, electrons, neutrals) of thermal plasma are in thermodynamic equilibrium and can be characterized by a single temperature. This temperature can vary from a few thousand Kelvin for plasma torch to more than a million Kelvin in fusion plasma applications and in the interior of stars.

In the second category, the average kinetic energy of an electron is extremely high in contrast to that of an ion. Plasmas that contain species that fit this description are called non-thermal glow discharges. Glow discharges can be easily produced inside powered reactors filled with a gas. Current conducting electrodes are generally used to increase the kinetic energy of the electrons through coupling with an electric field. For non-equilibrium (non-thermal) plasmas, the electron temperature is much higher than the mean ion temperature, which in turn is higher than the gas temperature, thereby giving access to high-energy electron-initiated reactions without accessing the high thermal gas temperature that can cause substrate degradation. In a non-thermal plasma, the electron temperature is much higher (10,000 K to more than 100,000 K) than the temperature of ions and neutrals, which are roughly the same and range from room temperature to about 2500 K.

The many and wide varieties of plasma applications depend on the mixture of ions, electrons, neutral and excited molecules, and photons that co-exist in the plasma.

1.3. Plasma process and technology

Chemically reactive plasma discharges are widely used for modification of the surface properties of materials. Plasma processing technology is vitally important to several of the largest manufacturing industries in the world. Plasma-based surface processes are indispensable for manufacturing of integrated circuits (ICs) used by the electronic industry. Such processes are also critical for the aerospace, automotive, steel, biomedical, and toxic waste management industries. Materials and surface structures can be fabricated that are not attainable by any other commercial method, and the surface properties of materials can be modified in unique ways.

The development of alternative ways of fabrication rises with the demand for advanced materials. Each year ever-smaller critical dimension is sought in the semiconductor industry. Old technologies such as photolithography and wet chemical etching process are unable to keep up with the manufacturing demands. Plasma on the other hand can remove and deposit materials used in the semiconductor industry with greater precision and control.

One of the examples of plasma used for material processing, are atmospheric-pressure plasmas. Many types of atmospheric plasmas sources have been developed in a wide range of frequencies from dc to microwave, or in a short pulse. For example, a microwave and RF plasma torch, a dielectric barrier discharge (DBD), an arc plasma torch, a capacitively coupled, atmospheric-pressure plasma jet are well-known examples of atmospheric plasma sources. In some application areas of atmospheric plasmas, especially for surface modification of large-area materials such as fabrics, polymers, or glass plates for liquid crystal displays or plasma display panels, having large plasma

volume or area with high uniformity in plasma parameters is one of the most important requirements that the plasma source should satisfy.

In arcs and torches, the electron and neutral temperatures exceed 3000 °C and the densities of charge species range from 10^{16}-10^{19} cm^{-3}. Due to the high gas temperature, these plasmas are used primarily in metallurgy. Corona and dielectric barrier discharges produce non-equilibrium plasmas with gas temperatures between 50-400 °C and densities of charged species typical of weakly ionized gases. However, since these discharges are non-uniform, their use in materials processing is limited. Atmospheric microplasmas provide interesting features that can address some of the limitation of current atmospheric plasma technology.

1.4. Introduction to atmospheric microplasma

Microplasmas are highly reactive and are of high electron density. These are key properties that make them well suited for production of new materials and application in advanced processing. Electrons are a key enabler of chemical reactions and their density and mean energy may be used to indirectly assess plasma reactivity [4].

Decreasing the size of the reactor that confines the microplasma enhances its non-equilibrium property. Taking advantages of this relationship (Fig. 1.1) and designing a system accordingly can generate "colder" plasma through decrease in the overall gas temperature and change in the energy distribution of plasma constituents. Microplasma non-equilibrium can be influenced without compromising reactivity and the ability to produce radicals.

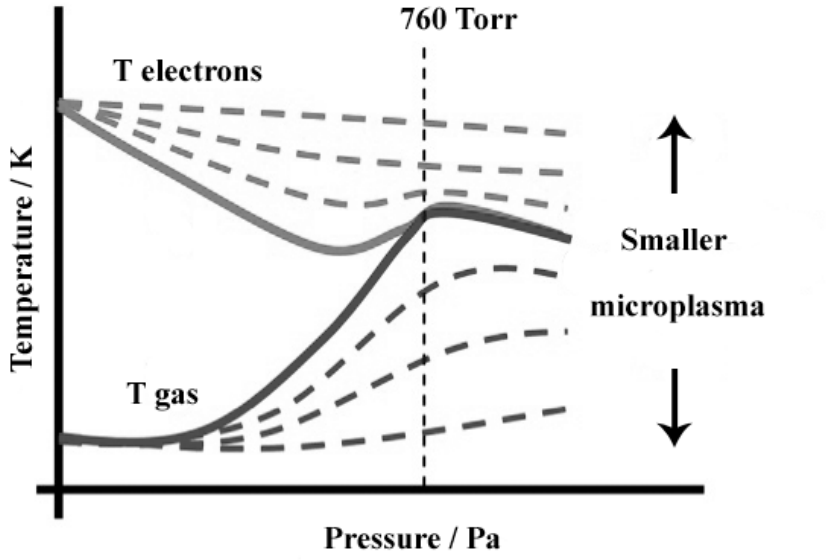

Figure 1.1 Non-equilibrium in small plasma cavities

Microplasmas obtained at 760 Torr are called atmospheric microplasmas. Ability to produce microplasma at atmospheric condition enables increase in manufacturing cost efficiency. This advantage makes processing with atmospheric microplasma competitive as well as complimentary in application.

The non-equilibrium nature of the atmospheric microplasma allows interaction with organic materials that produces no significant thermal damage. Properties that arise due to plasma's confinement promise to open a unique processing window. Both of these features of atmospheric microplasma can allow applications involving treatment of living cells and tissues such as high-precision plasma surgery, removal of cancer cells and cleaning of dental cavities [5].

Recently, an atmospheric-pressure microplasma jets has been developed, which exhibit many characteristics of a conventional, low-pressure glow discharge. In these, the

gas temperature ranges from 25°C-200°C, charged-particle densities are 10^{11}-10^{12} cm^{-3} and reactive species are present in high concentrations, i.e., 10-100 ppm. [6]

2. Fabrication of advanced materials

2.1. Introduction to nanotechnology and nanofabrication

Nanofabrication is a deliberately controlled manipulation and production of matter at the nanoscale (1 to 100nm). This manufacturing practice is aimed to create materials, devices, and systems with fundamentally new properties and functions.

Currently, the need for new materials is high in medical, optical and semiconductor industries. One of the ways to address this demand is through practices put forth by nanotechnology. To keep up with the creed of semiconductor industry of producing smaller features at a faster pace and reduced cost in accord with Moore's law, investment into alternative fabrication must be made. Nanotechnology is thought to enable the microelectronic industry with methods of uncapping the limitation modern world is currently facing in small feature manufacturing. Atmospheric microplasma is theorized to be a feasible technology for production of nanostructured materials.

2.2. Overview of nanostructured materials

2.2.1. Carbon-based materials

One of the most studied carbon based materials is carbon nanotubes. Carbon nanotubes are tubular allotropes of carbon and are one of instances of nanostructured matter currently pursued by industry. They are formed when carbon atoms are tied along a cylindrical surface and bonded by sp2 chemical bonds in an organized manner. This

compound is stronger than diamond formed by sp3 chemical bonds and is similar in composition to graphite.

Carbon nanotubes can be said to possess an inherent nanostructure. Advanced processes and technologies are required in order to arrange the chemistry of the carbon nanotubes in this way. The difference between the graphite and carbon nanotubes is that of structural geometry where graphite can be thought of a sheet like carbon arrangement and nanotube is cylindrical.

Generally for production of carbon nanomaterial such as carbon nanotubes, carbon feedstock and a metal catalyst that triggers organized growth are required. Once these ingredients are properly treated the end product can show nanostructured characteristics. The most common way to synthesize carbon nanotubes is to introduce a relevant amount of carbon feedstock into a heated chamber or plasma. This can enhance disassociation of hydrocarbon ions, resulting in radicals that can be employed in forming nanotubes. Carbon nanotubes are produced when carbon radicals agglomerate at the surface of catalyst particles that must be present at the target where carbon nanotubes growth is desired. Another way to synthesize carbon nanotubes is inside the plasma containing both the catalyst and reactive carbon species. The nanotubes can then be precipitated onto the target surface.

Usually, for production of carbon nanotubes various types of feedstock gases are used. Methane CH_4 or acetylene C_2H_2 can be decomposed into ions that can disassociate into carbon rich radicals. Liquid vapor of organic solutions can also be decomposed to give similar reactive species. A liquid mixture of ferrocene powder and xylene serves as source of both, the carbon feedstock and metal catalyst. Ferrocene is a great powdery

source of iron catalyst. Dissolving it in xylene, a carbon containing organic solvent produces a volatile liquid. When this liquid is heated to temperatures close to its boiling point, the vapor pressure of this fluid is overcome. The vapor produced in result can be added to the plasma discharge previously initiated. One of the advantages of using system that incorporates the latter is its ability to provide the catalyst along with the carbon feedstock.

The latter mechanism is known to open up possibilities of "in-flight" catalyst treatment that accommodates for synthesis of carbon nanotubes inside the plasma reactor and deposits the catalyst particle along with the carbon material.

The other way is based upon the activation of the catalyst already deposited on the substrate. This process triggers the growth of nanostructures outside the reactor and on the surfaces that come in contact with the plasma. To produce carbon-based nanocrystaline materials, heated catalyst must be submerged into a jet of plasma containing radicals necessary for self-assembled growth of carbon nanostructure. The electrodes used to generate plasma can serve as a substrate for carbon deposition.

Both processes require the presence of carbon feedstock within the plasma but differ in the location where the metal catalyst initiates the nanotube growth. The gas initially ionized is usually Ar or He. Such gas is called a carrier gas since it serves as a buffer for subsequent chemistry introduction as well as a source of energy for feedstock decomposition. Inert gases are selected because they are not reactive and generally safe to work with under most conditions.

In both cases, the surface area of the catalyst is the factor limiting the volume of the carbon nanotubes grown. Fine tuning the diameter of the catalyst particle is an important practice that requires meticulous attention for a successful deposition result. Finely tuned ratios of involved chemicals and ionizing energies can trigger multitude of wanted and unwanted disassociation processes. Selecting the appropriate ones is the key for depositing a nanostructured material.

2.2.2. Nanocrystaline metal oxides

Nanocrystaline metal oxides are important because they offer a number of unique electrocromic, photochromic and optical properties. Molybdenum oxide for example are recognized as a promising material for a rapidly increasing number of applications including, e.g., chemical synthesis, petroleum refining, sensors, optoelectronic devices, catalysis, smart windows, display, supercapacitor and battery applications [7]. Using microplasma, particles of nanocrystaline oxides can be formed with low processing temperatures. If the discharge parameters are tuned properly the shape and size of the resultant nanoparticles can be controlled. Oxygen and source of metal atoms must be present within the discharge that is used for substrate processing.

Metal oxides find use in many applications, for example systems for photochemical splitting of water into H_2 and O_2 molecules are based on TiO_2 catalysts. Such systems usually employ solar energy in order to be powered [8].

Nanocrystaline metal oxides find use as transparent conducting oxides as well as in gas sensor material. For example, SnO_2 nanoparticles are extremely important sensor material practical for detection of leakage of inflammable gases due to their high sensitivity to low gas concentration [9].

Battery electrodes made from Ni and Mo oxides can increase battery's electrochemical capacities and increase charging rates [10], [11].

3. Description of atmospheric microplasma system

3.1. System overview and design

System capable of generating atmospheric plasmas is assembled. This system is adaptable to some of ways currently investigated by the scientific community to produce crystalline carbon-based materials and metal-oxide nanostructures. To understand whether they are capable of generating and sustaining a microplasma, a preliminary classification of its competence is carried out. Such initial study allows exploration of operating conditions of the system and finding approximate parameters for nanofabrication.

The entire system is fairly complex however a number of major components can be clearly distinguished. Fig. 3.1 conveys the way these components interact and the overview of the system can be seen in Fig. 3.2. Unlike, any other block, plasma reactor is the only block easily swappable. The rest is permanently in place to service the plasma reactor.

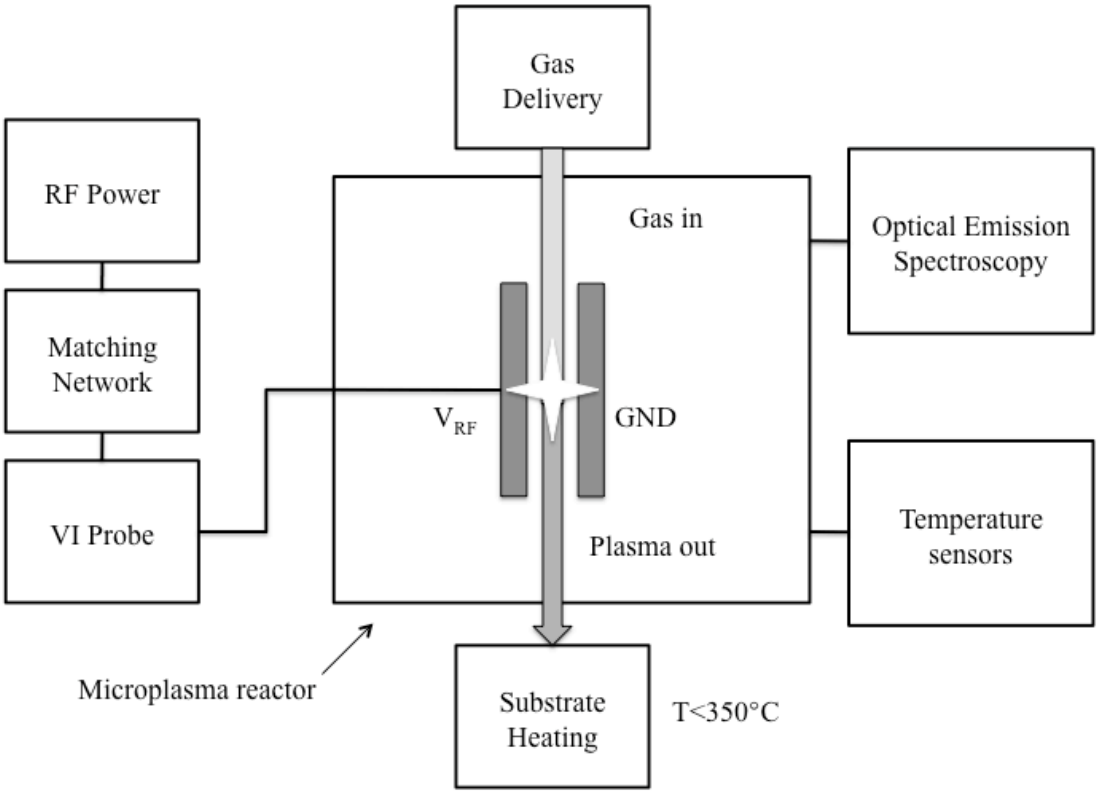

Figure 3.1 Diagram of the experimental setup

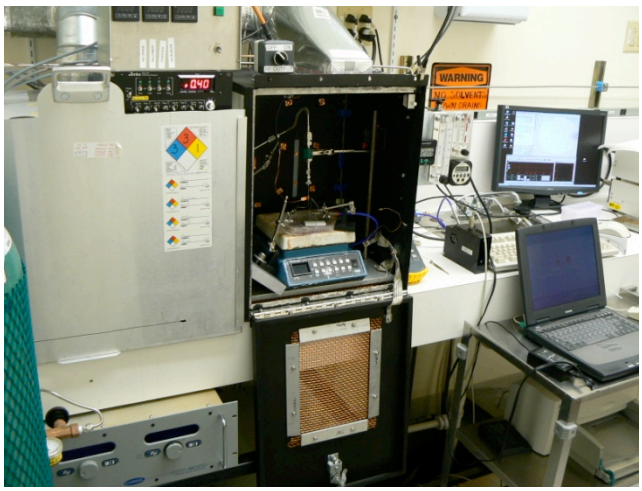

Figure 3.2 Photograph of the experimental setup

Plasma discharges operating at atmospheric pressure are generally driven by sinusoidal voltages at frequencies ranging from 50 Hz up to RF and microwaves. [12] To address this design requirement, the system is based around 13.56 MHz radio frequency (RF) power source shown in Figure 3.3.a. Only one of the generators of this dual unit is used to power the plasma reactor. The lowest power that can be supplied by this source is 10 Watts. The maximum of 2000 Watts allowed can be stepped up by increments of 5 Watts. Since, the goal of this development is to produce a system that is also power efficient only lower ranges of power are explored. Also, higher power may not be suitable for generation of non-thermal stable discharge.

An automatic matching network (Fig 3.3.b) is used to manage the electrical power delivered from the power generator to the plasma reactor. When the system is operational, this unit adjusts its internal impedance to match the 50 Ω impedance required to minimize the reflected power. The matching can be accomplished in two ways: manual and automatic. Automatic matching uses algorithms in order to accommodate the complex impedance while manual matching is used for fine-tuning of unstable glow discharges and when automatic matching fails.

For characterization purposes the amount of power is monitored with V-I probe and impedance analyzer. This instrument shown in Figure 3.3 (c), (d) allows measuring and logging voltage-current characteristics of the plasma as well as its complex impedance. Using this instrument electrical data is collected based upon which information about the regimes of plasma, attainable by this system, is derived.

Figure 3.3 Power block a) CDX-2000 13.56MHz Dual RF Generator b) automatic matching network c) VI probe d) impedance analyzer

The distribution and mixing of the gases and their delivery to the plasma reactor is accomplished through a network of piping, plumbing fittings and valves managed by four mass flow controllers and a readout unit (Fig 3.4.a, b). The plasma chemistry, apparent due to the decomposition of the precursor inside the reactor, is a result of the incoming flux of the gases that an operator selects at the readout unit

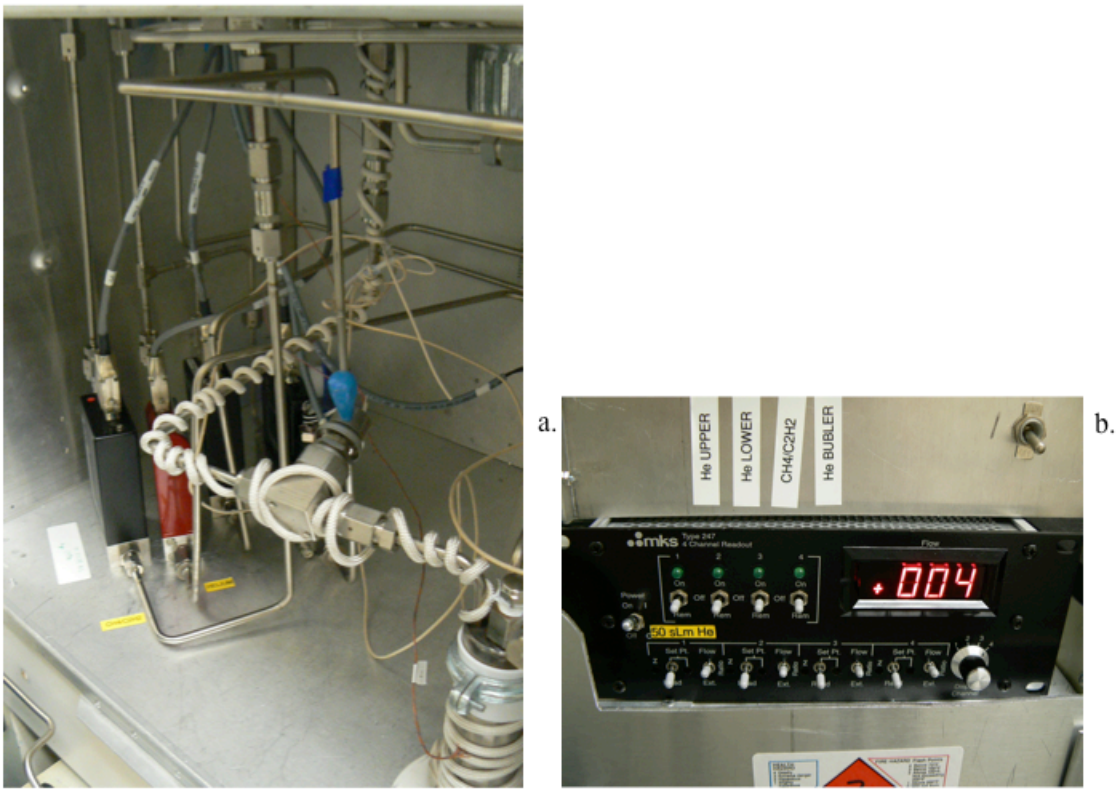

Figure 3.4 Gas distribution block a) Mass flow controllers b) readout unit

This gas delivery system also includes a 294 cm^3 bubbler (Fig. 3.5.a) that is used for evaporation of liquids and water. Heating the bubbler containing a volatile solution produces vapor that can be used as a precursor gas for deposition. Using a bubbler is a potential for generating hydrogen and oxygen ions. Boiling water can provide a source of hydrogen that could be ionized within the reactor. Water can also serve as a source for oxygen for oxidation of metals for metal oxide deposition. The gas lines and the bubbler are heated using line heater that was put together for this study (Fig. 3.5.b). This self-adjusting unit assists in production of vapor precursors.

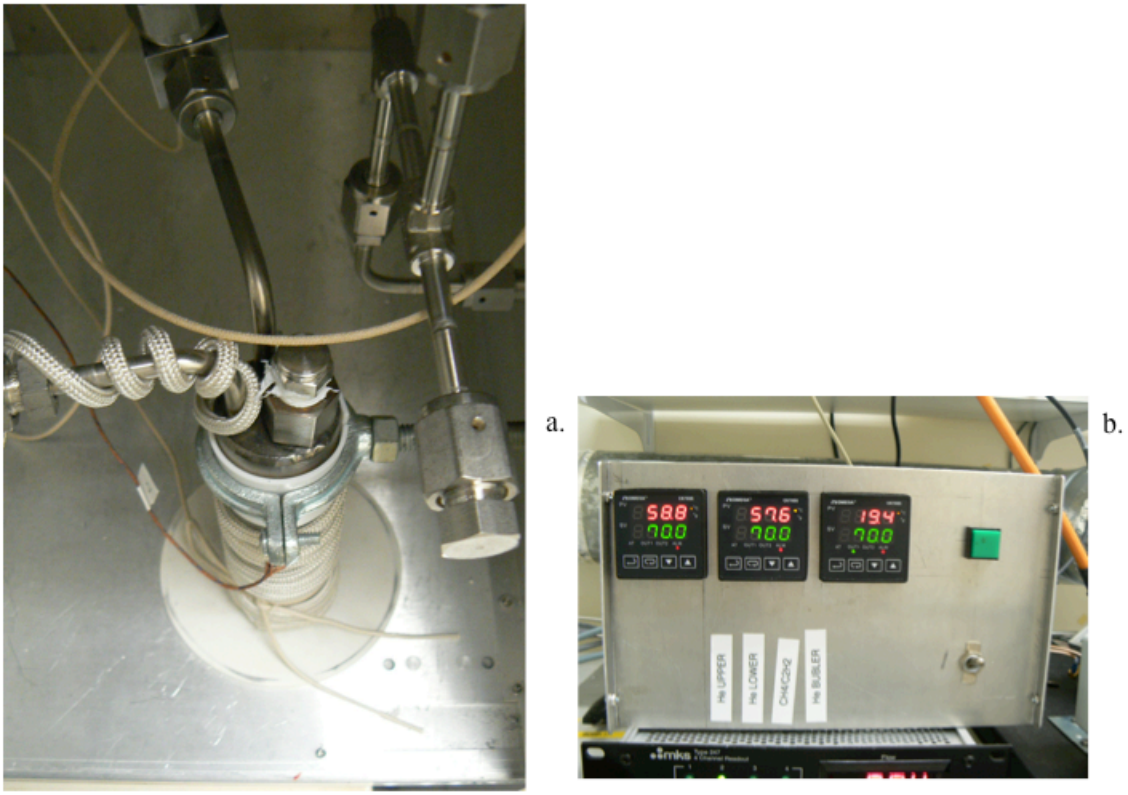

Figure 3.5 Gas distribution block a) bubbler b) line heater

The placement of the plasma reactor in relation to the substrate can be adjusted using a micropositioner shown in Fig. 3.6. This device allows controlling the distance between the reactor and the target substrate.

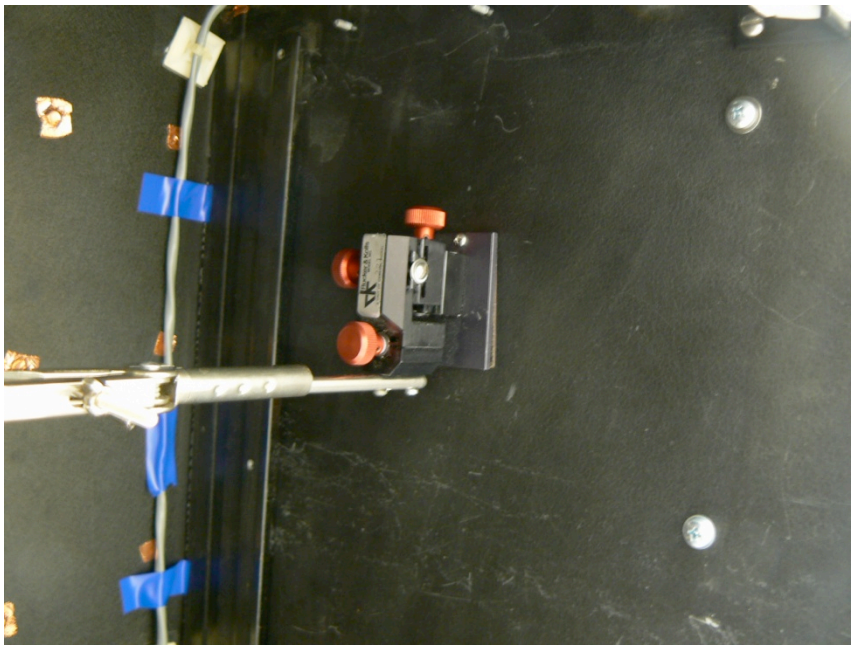

Figure 3.6 Micropostitioning manipulator

In order to assist the dissociative and formative processes at the sample's surface a hot plate (Fig. 3.7) is used to control the substrate's temperature. Using this unit temperature below 350 °C can be attained.

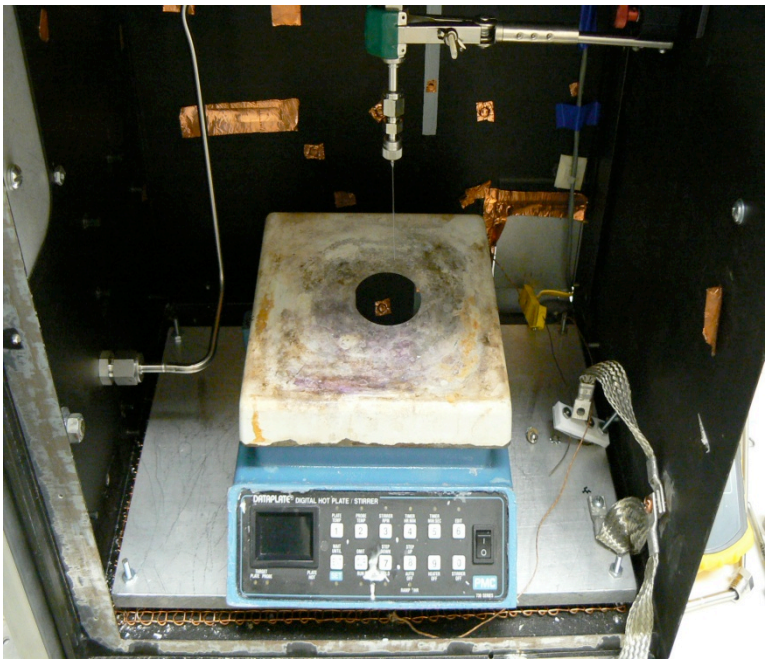

Figure 3.7 Hot plate

3.2. Microplasma reactors

Four types of microplasma reactors are considered in this investigation. These can be swapped around and are application specific. The first type of reactor called "linear plasma head" (LPH) was mainly used for basic investigation of the microplasma regime. The other three types have been used for nanofabrication. These reactors were designed in such a way that they integrate with the power and gas components previously described with minimal system adjustments.

3.2.1. Linear plasma head reactor

This reactor is of planar geometry and consists of two parallel aluminium plates separated by sub-millimeter distance. For the purpose of investigating microplasma, this distance, also referred to as the electrode spacing, can be varied. The maximum electrode distance that can be achieved through an adjustment is about a couple of millimeters and

the minimum is around 100 μm. The minimum distance is dictated by the surface roughness of the aluminum plates. The presented investigation for this reactor was carried out only for distances inside 100-800 μm range.

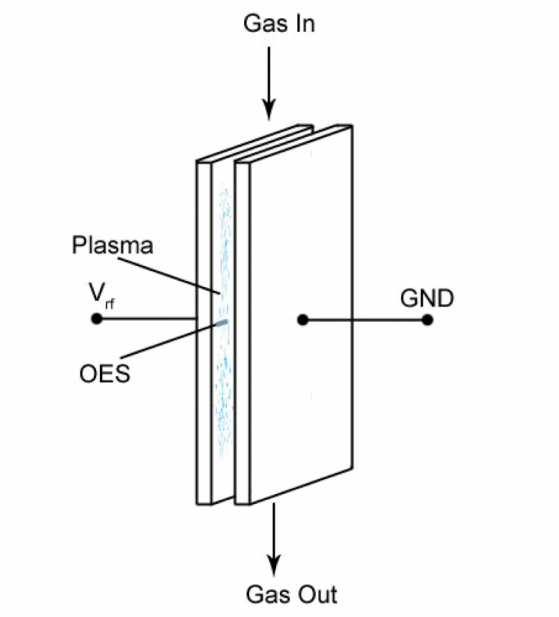

Figure 3.8 Working principle of a linear plasma head

The electrode width and length are fixed at 5 and 10 cm respectively. Current and power densities established in the reactor can be estimated using the surface area of the electrodes and the current flow through the plasma.

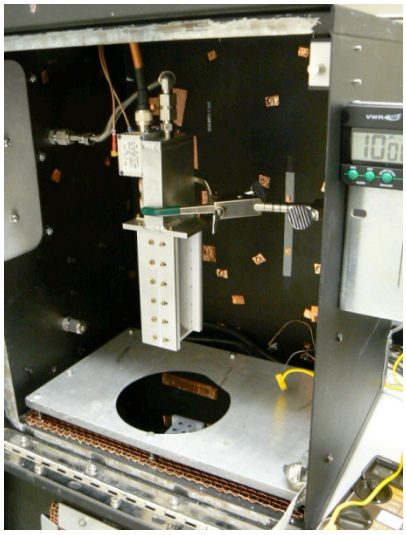

Figure 3.9 Photo of linear plasma head

With the ability to measure the voltage-current characteristics of the plasma, other plasma characteristics such as the thickness of the plasma sheath can be calculated. This reactor is well fitted for investigation of the microplasma regime.

In this setup electric field needed to ionize gas is established perpendicular to the gas flow. It is worthwhile of noting, that this reactor allowed mixing of relatively large volumes of gases. The gas-mixing scheme for this reactor is shown in Fig. 3.10. This demonstrates the constraints put on this reactor by the gas equipment as well as the range of available gas combinations. The difficulty of the characterization of this setup is not only limited to the large number of possible gas combination. Factors such as electrode spacing and applied power also play a significant role and must be also included in the consideration. Before the investigation of the properties of the plasma could be carried out only those parameters are selected that produce a stable plasma discharge.

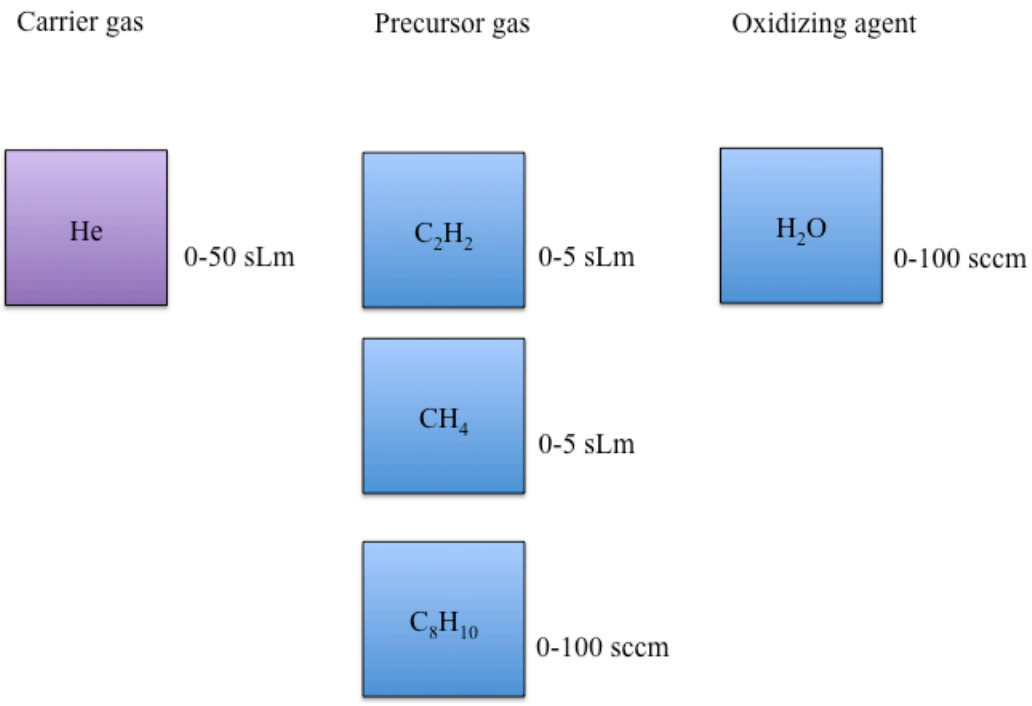

Figure 3.10 Gas mixing in linear plasma head

3.2.2. Capillary plasma reactors

This type of reactor is formed inside of a needle-like assembly and is a subject to number of unique ways in which it can be powered. The design of the reactor is based on concentrically nested quartz and metal cylindrical tubing and wire. In particular three configurations that adapted three different powering schemes are explored. These are tube-ring (Fig. 3.11.a), ring-wire (Fig. 3.11.b) and patch-tube (Fig. 3.11.c).

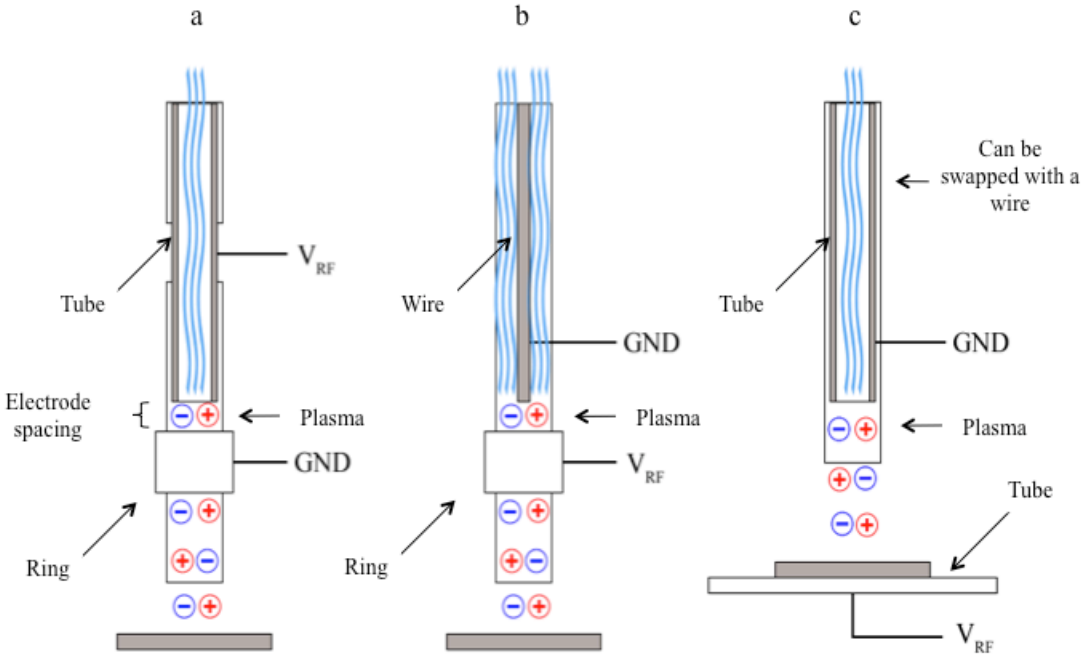

Figure 3.11 Powering schemes of microplasma reactors a) tube-ring, b) ring-wire, c) patch-tube

In the first two configurations, the assembly is inserted into a copper ring electrode and is put together in such a way that the ring's edge is at a distance from the end of the inside electrode. Plasma is generated within the electrode spacing and this

distance is comparable to electrode spacing of the linear plasma head. Depending on the configuration, the ring can serve as either the powered or the grounded electrode. The gap between the electrodes can be adjusted using the micropostioning manipulator mentioned previously in section 3.2.

The first two arrangements allows generation of Ar-based plasmas. No argon microplasma can be generated using the linear plasma head set up since it does not allow to decrease the electrode spacing sufficiently to small dimension at which the ionization energy is efficiently distributed among the plasma constituents.

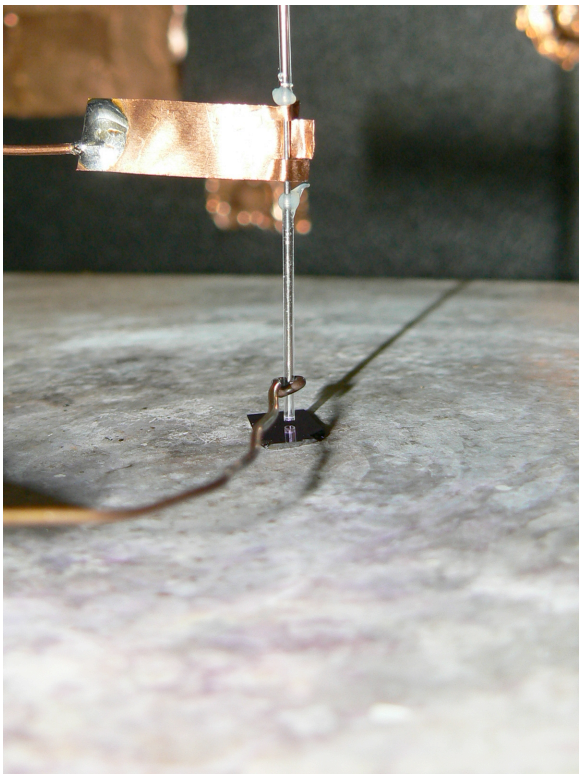

Figure 3.12 Photo of capillary reactor with tube-ring powering scheme

By investing into quartz capillary of different diameters reactor size can be altered. Different metals and diameters can be used for the tube electrodes. For the ring-wire configuration, the wire-electrode gauge and composition can be varied as well. Capillary plasma reactors are disposable and offer advantages for nanofabrication in

comparison to the linear plasma head since they address the issues found with linear model described in the nanofabrication section of this report.

These reactors can be started with low volumes of gas mixtures (< 20 sccm) and small amount of applied power. Since power and gas are conserved, the advantage of these assemblies for thin film production is noted. However, gas flow to area coverage must be investigated. In the ring-wire configuration, radicals are produced by decomposition of the wire's surface and are used for deposition at the remote substrate. The wire can be of different composition and gauge hence yielding various plasma chemistries. Molybdenum, nickel and titanium are examples of some metal that were investigated for the ground electrode compostion.

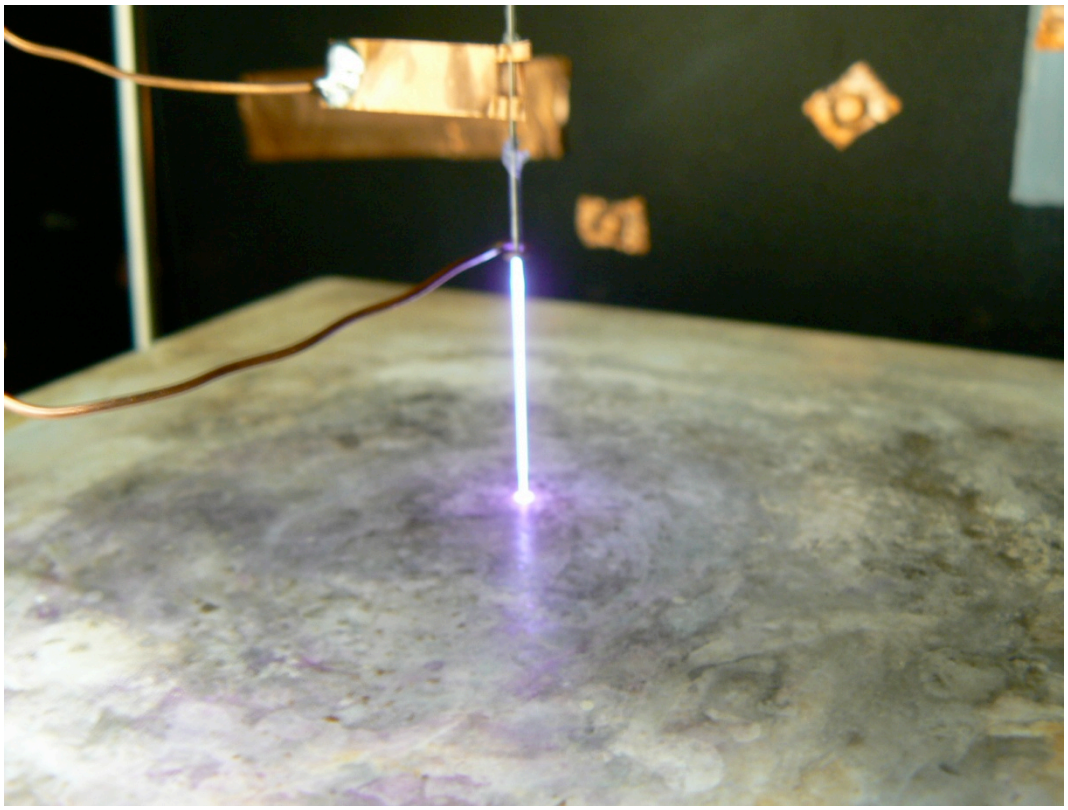

Figure 3.13 Capillary plasma reactor in operation

For this study, quartz tubing of 700 µm inner diameter and of 300 µm wall thickness was used. Nickel is chosen to be the material of the inner tube electrode. The available inner tubing diameter is 150 µm with wall thickness of 450 µm.

Since this reactor is fragile and the electrode size only allows ionizing small volume of gas, mass flow controllers only of small resolution can be used. The complexity of the mixing scheme shown in Fig. 3.13 provides innumerable amount of recipes that expands as factors such as experiment time, electrode spacing, plasma power, electrode composition are considered.

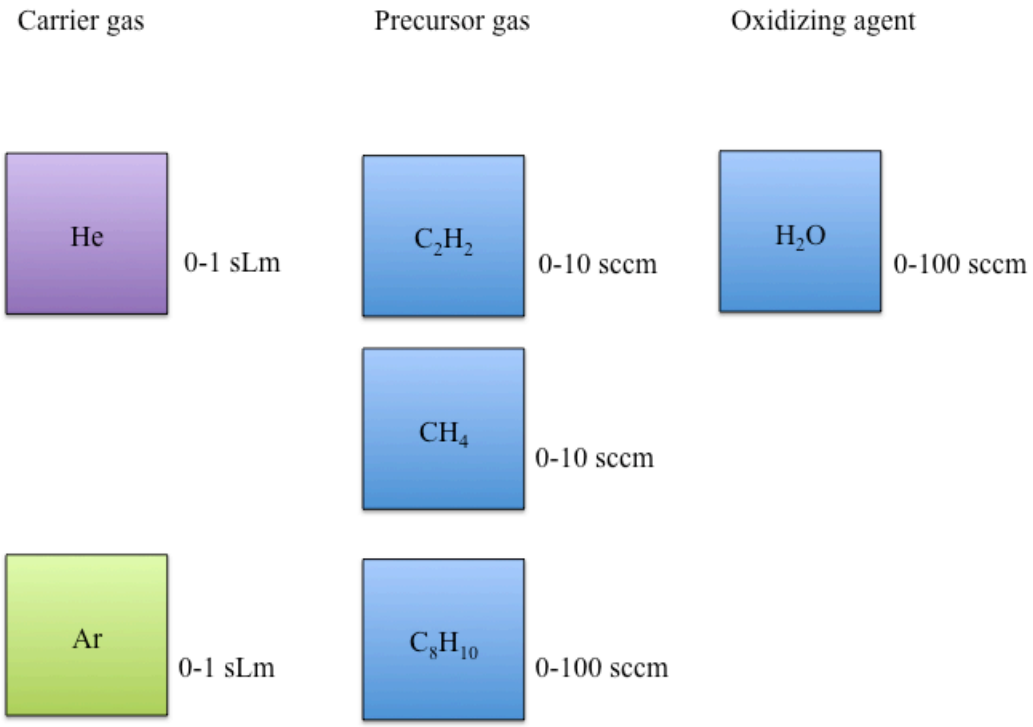

Figure 3.14 Available gas flows for capillary reactors

3.3. Diagnostics

A range of stable plasma operation parameters can be established for various plasma chemistries produced inside the reactors. Flow of the current through the gas can be controlled by application of voltage. Knowing the voltage and current characteristics of plasma can help determining electron temperature and density that are useful for plasma characterization. The electrical characteristics of the produced plasma is measured by the V-I probe which was described previously.

Producing V-I curves for different discharges is not the only way to study the characteristics of the plasma discharge. Another method available for this study is spectral characterization or optical emission spectroscopy (OES). This technique is relatively inexpensive and convenient means of studying plasma. Qualitative overview of plasma composition can be obtained quickly from line/band intensities and some more elaborated analysis can provide information about various excitation/ionization processes and temperatures in the plasma. It is important to note that controlling the deposition process by monitoring the optical emission of particular species can allow obtaining good reproducibility of the undertaken deposition process [13].

Concentrations of reactive species can be characterized. Detection of impurities within the plasma discharge can also be investigated using this technique. For instance, when the gas flow rate is low, air leaks into the reactor. Its content must be investigated since it has an effect on the breakdown voltage of the gas and thus on consequent plasma behaviour. Leakage of air in the system can be detected from the emission intensities of Nitrogen bands.

Finally, temperature probes have been used to measure and monitor the gas temperature at the outlet of each plasma reactor and at the substrate.

4. Basic plasma characterization

4.1. Investigation of the microplasma regime

The basic investigation of microplasma properties is carried out using the linear plasma head reactor

In theory, when a plasma discharge is produced two main regions are formed. One is a region of high space charge gradient called sheath. The other is the plasma's bulk. Sheath develops at the surface where plasma interacts with an electrode. It is a positively charged layer and mostly made up from ions. The bulk of the plasma consists of neutral gas molecules, electrons as well as other species. When a plasma discharge is produced between two electrodes, two sheath regions are developed and the bulk plasma is contained between them (Fig. 4.1).

As long as the sheath thickness is adequate, electrons can reach the gas ionization energy and create new electron-ion pairs that assist in sustaining a stable plasma discharge. When the electrode spacing is significantly large the developed sheath is fully formed and its characteristics depend solely on the current density at the electrode. The thickness of the bulk region is dependent on the variance in the electrode spacing. Increasing the current density of the discharge decreases the sheath thickness and increases the size of the bulk.

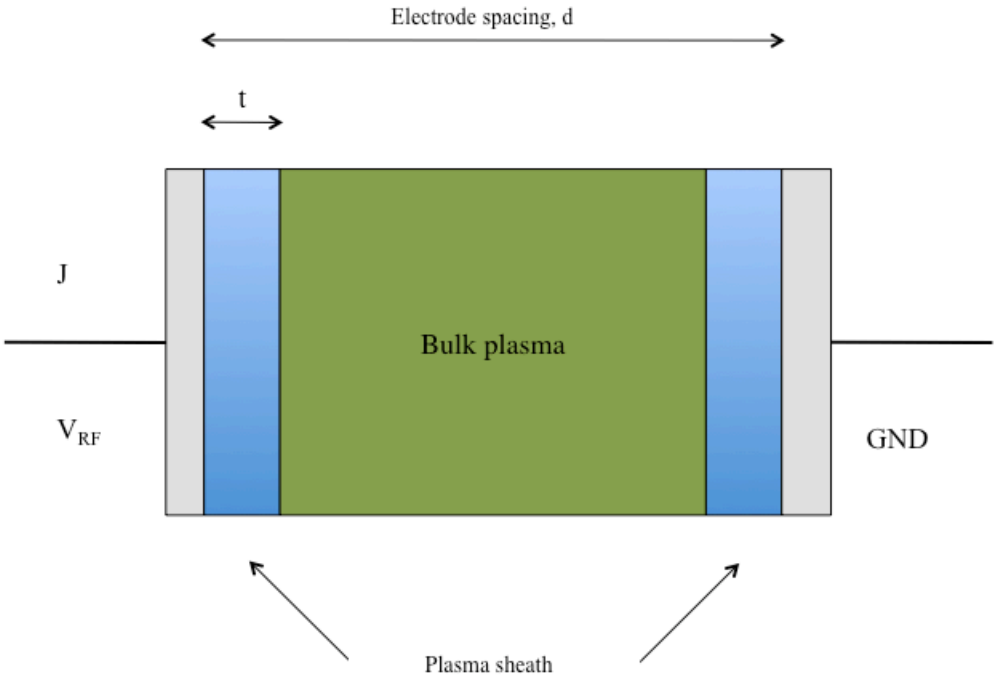

Figure 4.1 Glow discharge region formation

Usually, the thickness of the sheath is fixed and independent of the electrode spacing. However, it has been observed that shrinking the distance between the electrodes containing the bulk can also affect the sheath structure in some cases. Decreasing this distance to dimensions comparable to the thickness of the sheath can prevent the full development of the regions' structure and give plasma unique characteristics. When the electrode distance is decreased, the electron trapping is weakened and the discharge structure deviates from the basic sheath-bulk composition of glow discharges and their physical properties depart from the conventional discharges produced under atmospheric pressure [4].

In our experiments at sub-millimetre electrode spacings, we have observed that the sheath structure is dependent on the dimension of the plasma confinement indicating a transition to a new regime with unique characteristic features. This regime is what we call a microplasma regime.

To investigate microplasma properties, current and voltage of the discharge were measured and the relationship between the two was plotted in Fig. 4.2. In this figure, the two types of atmospheric glow are apparent. It is evident that for the electrodes spacing that falls within the range from 500 to 800 μm, the voltage developed across the sheaths is independent on electrode the separation. The voltages developed in the discharge produced in the linear head with electrode spacing of 500, 600, 700 and 800 μm did not vary by much. However, as the electrode distance was decreased to smaller distances a change in voltage behavior is observed and it follows the spacing scaling. The voltages developed for 100 and 250 μm electrode spacing do not consolidate in the similar region of the graph showing a transition of the classic atmospheric plasma to atmospheric microplasma.

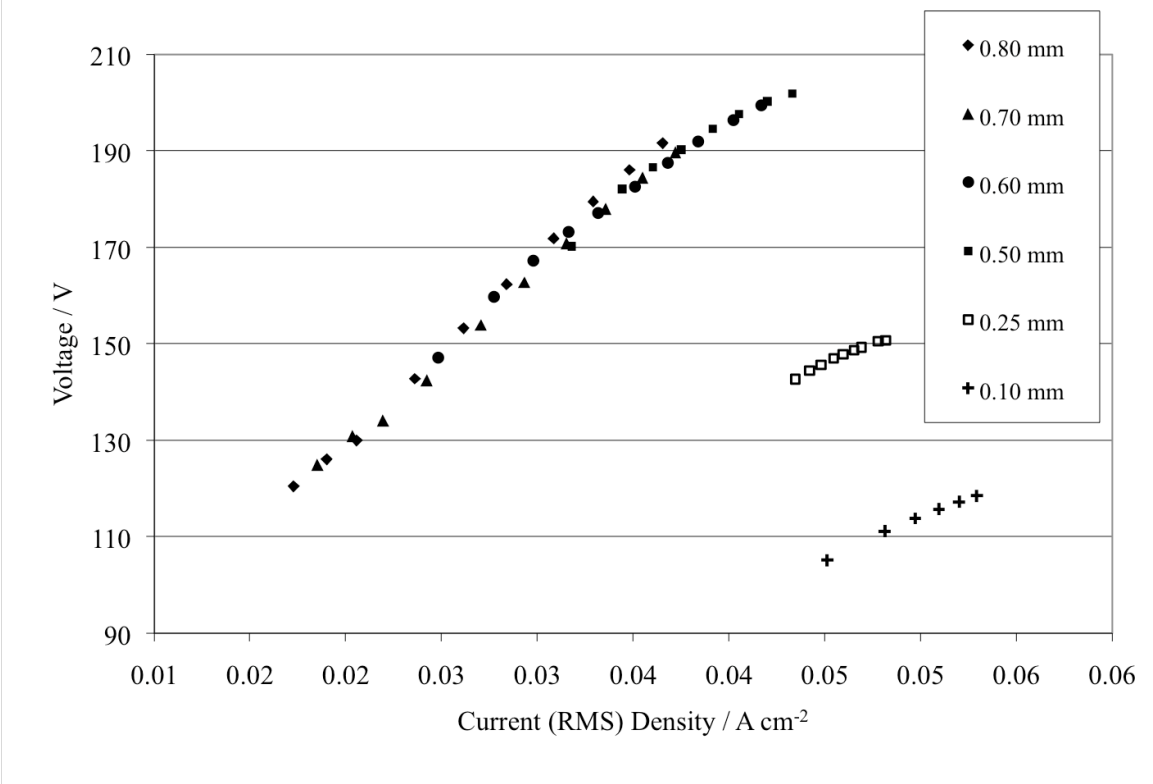

Figure 4.2 Voltage developed across plasma discharge

RF plasma bulk and sheaths can be characterized by their thickness, voltage and electric field. Bulk is the resistive component of the plasma where sheath is the capacitive one. The thickness of the sheath can be determined since the geometry of the electrodes is known and the capacitance of the plasma is determined with the V-I measurements. The capacitance of a parallel-plate capacitor can be estimated using

$$C = \varepsilon \frac{A}{d},$$

where A is the area of the electrode, and d is the thickness of the sheath. It is assumed that the permittivity of the sheath, ε, is that of vacuum. Since, both the capacitance and the area of electrodes are known the sheath thickness can be estimated for the plasma

produced in the LPH reactor with different electrode spacing if it is assumed to behave as a capacitor.

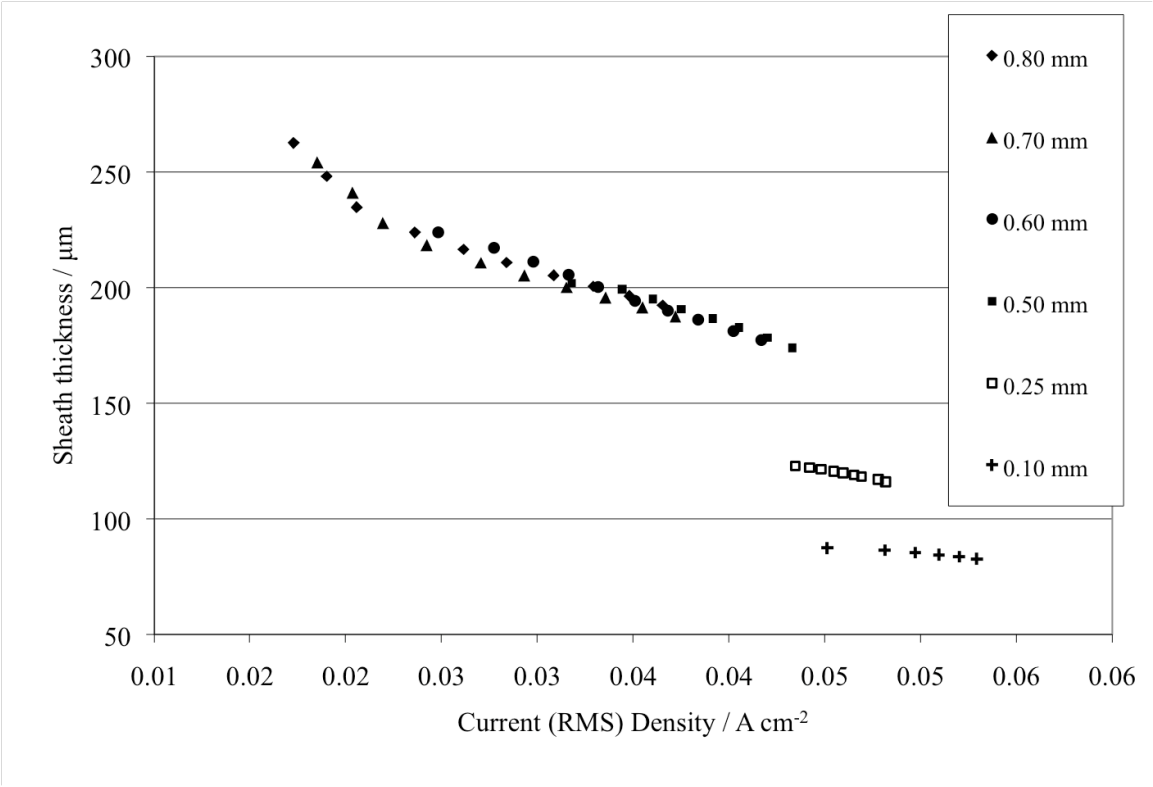

Figure 4.3 Developed sheath thickness

Using Fig. 4.3, it can be concluded that for a given electrode gap, the partition of the bulk and sheath plasma regions depends on current density. The sheath thickness is found to diminish with the increase in current density. The effect of the electrode gap on the disruption of the sheath-bulk equilibrium is found to take place when the electrode gap employed has fallen to smaller sizes, 100 µm and 250 µm.

The development of the electric field across the bulk can be also calculated. The bulk size can be determined by subtracting the known sheath thickness from the electrode spacing. The voltage across the bulk can be determined by considering the Ohm's law.

The current though the plasma is constant and at the bulk it is equal to the current developed between the electrodes as the voltage is applied. This value is determined by the measurement with the V-I probe. The bulk is the resistive component of the plasma and its resistance is the real part of the complex impedance of the plasma. Since the V-I probe can measure, the magnitude and the phase of the impedance, the resistance of the bulk can be calculated. A number for the voltage developed across the bulk can be found, once the determined resistance is multiplied by the developed current. The electric field is found by dividing the voltage established across the bulk by its width.

In Fig 4.4, curves produced for gaps lower than 250 μm are overlapping. The electric field developed across the bulk was found to be highest at smaller electrode distance. However, when the gap was sufficiently large the electric field developed across the bulk was independent of the electrode spacing. Higher electric field cause electrons to obtain higher kinetic energy thus making plasmas more reactive.

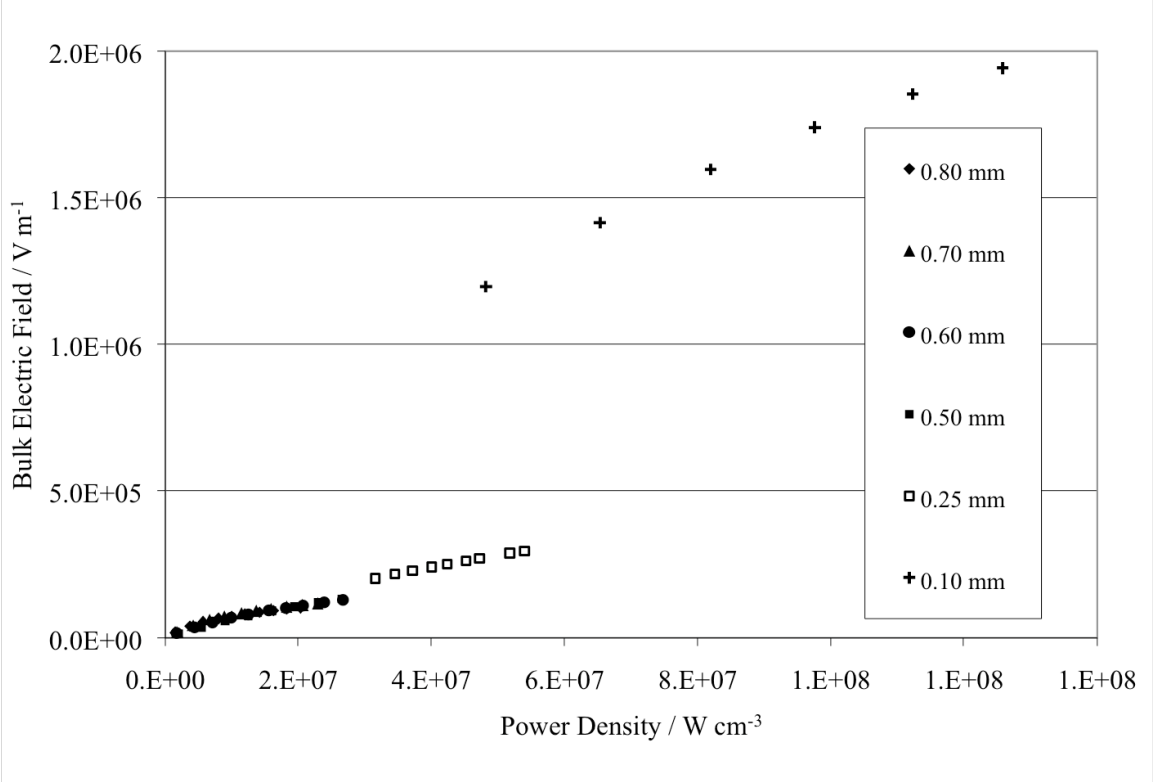

Figure 4.4 Electric field across the plasma bulk

In order to obtain an informative result for this study, only constant gas velocities are considered. The flow of the gas through the reactor therefore is scaled in such a way that the velocity remains steady. During the experiment, the flow rate is regulated to reflect the adjustment in the electrode spacing.

4.2. Gas temperature measurement and verification of non-equilibrium

To confirm that the generated microplasma was non-thermal, temperature measurements of the effluent were taken. The data was collected for both linear plasma head and capillary reactors.

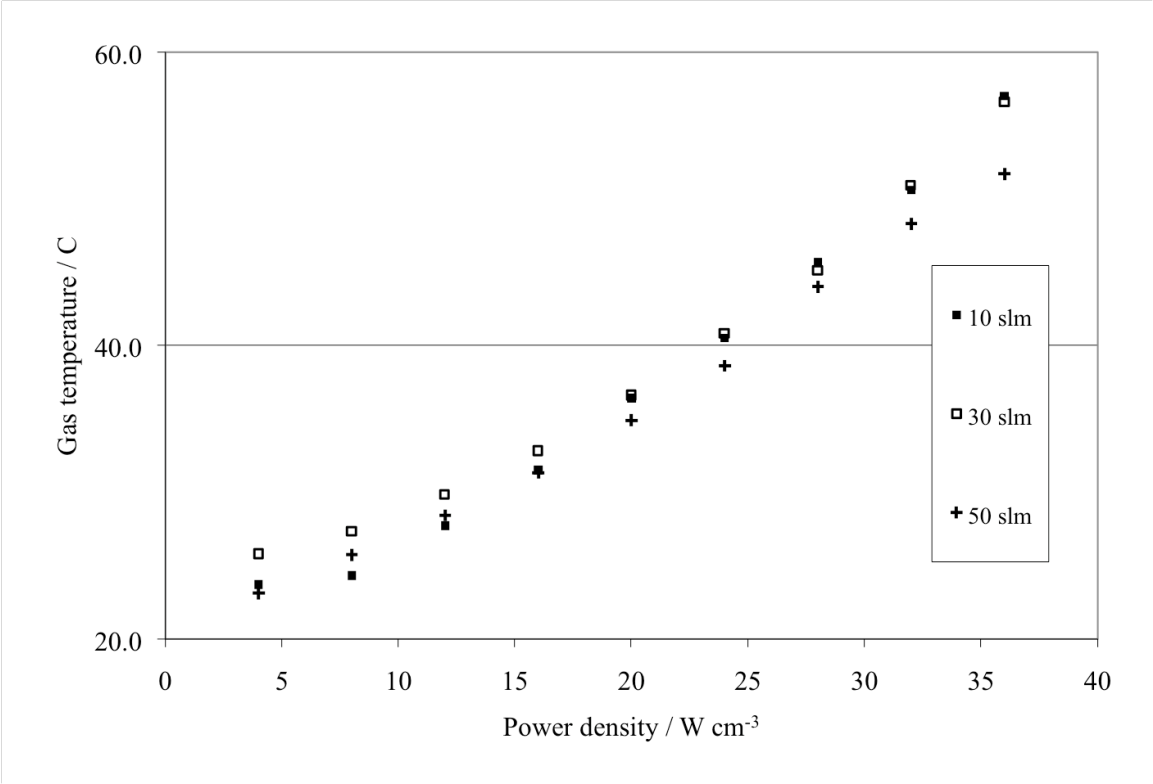

Figure 4.5 Helium effluent temperature measurements in linear plasma head

Fig. 4.5 demonstrates an approximation of linear behavior observed in the relationship between the applied power and the developed gas temperature in helium plasma produced in linear head. Changing the gas velocity did not produce any significant deviation in temperature characteristic and the temperature value obtained at different power densities were similar for different gas flows. Light emission was observed leading to conclusion that electrons acquired enough of kinetic energy to produce excited states that were able to relax and emit photons. This was also confirmed by the data collected with OES. Overall, gas temperature was low and the plasma generated in linear head was considered non-thermal.

Argon glow could not be produced successfully inside the linear plasma head even at smallest gap resolution used for helium. Ionization/excitation of helium and argon occurs in different ways and this can explain the circumstance. Energies needed to ionize and to excite helium are fairly close. However, argon ionization is a significantly more complicated process than that of helium. The energy usually spent for ionization also must accommodate most of the possible ways of excitation before the discharge is produced. In helium plasma, this is achieved more readily than in argon. However, the capillary setups were able to address this challenge. It is reasonable to note that helium is more expensive than argon that is why it is not preferred for manufacturing

Since the capillary reactor was designated for manufacturing, argon plasma was considered and measurements were taken when stable discharge was produced. For this reactor low gas flow was considered (150 sccm) and the powering scheme investigated was tube-ring. It was assumed that the other powering schemes would produce similar results since the amount of power used for powering the reactor did not vary between the configurations.

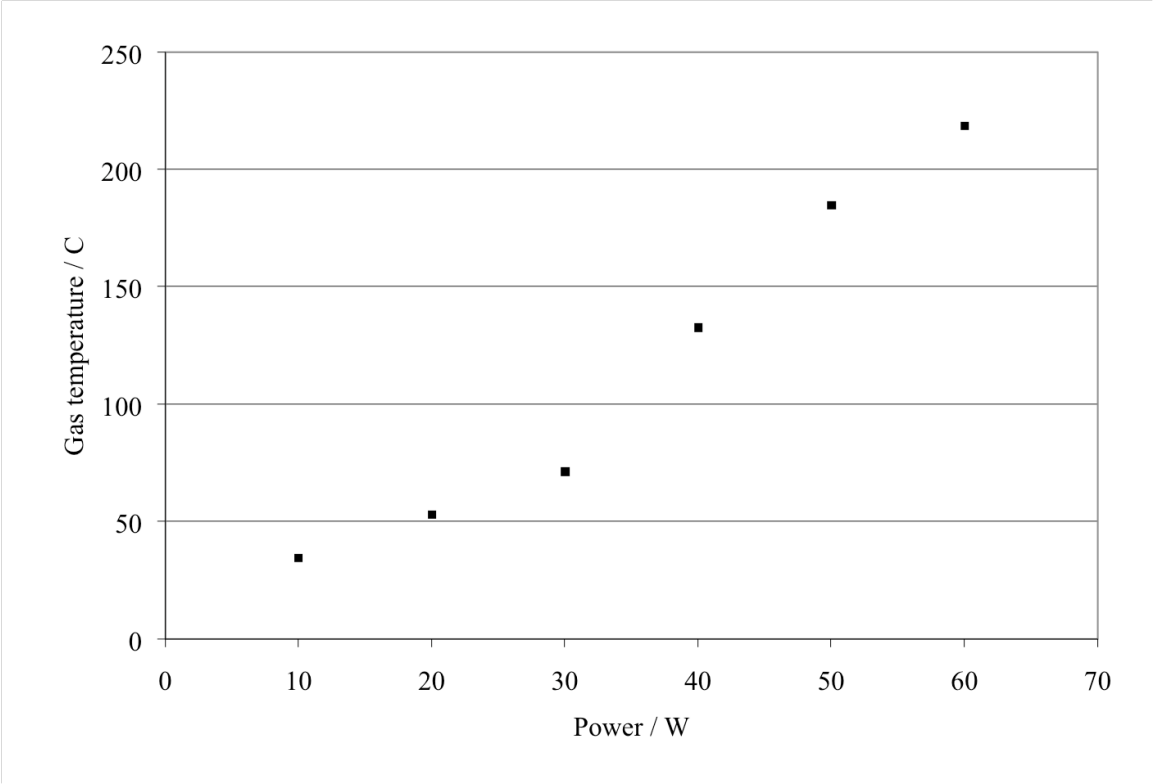

Figure 4.6 Argon effluent temperature measurements for capillary setup

Capillary plasma reactor was able to produce non-thermal plasma. Fig. 4.6 shows linear increase in gas temperature with of supplied power. Rapidity in the increase of the gas temperature was explained due to contribution from the resistive heating of the powered electrode. The gas temperature was found to be linearly dependent on the power applied to the gas. Each value was obtained as the temperature stabilized over time. Helium data could not be collected due to unexpected electrical interference of the temperature probe with the electromagnetic field of the plasma.

4.3. Effect of precursor plasma non-equilibrium

It was observed that addition of methane precursor to helium plasma generated inside the linear plasma head had no significant effect on the developed gas temperature. Different mixture ratios have been investigated and the linear relationship between the applied power and the temperature was preserved. Fig. 4.7 provides the data for the temperature measurements carried at the outlet of the reactor when 0.5 vol%, 1.0 vol%, 1.5 vol%, and 2.0 vol% methane/helium mixtures were ionized.

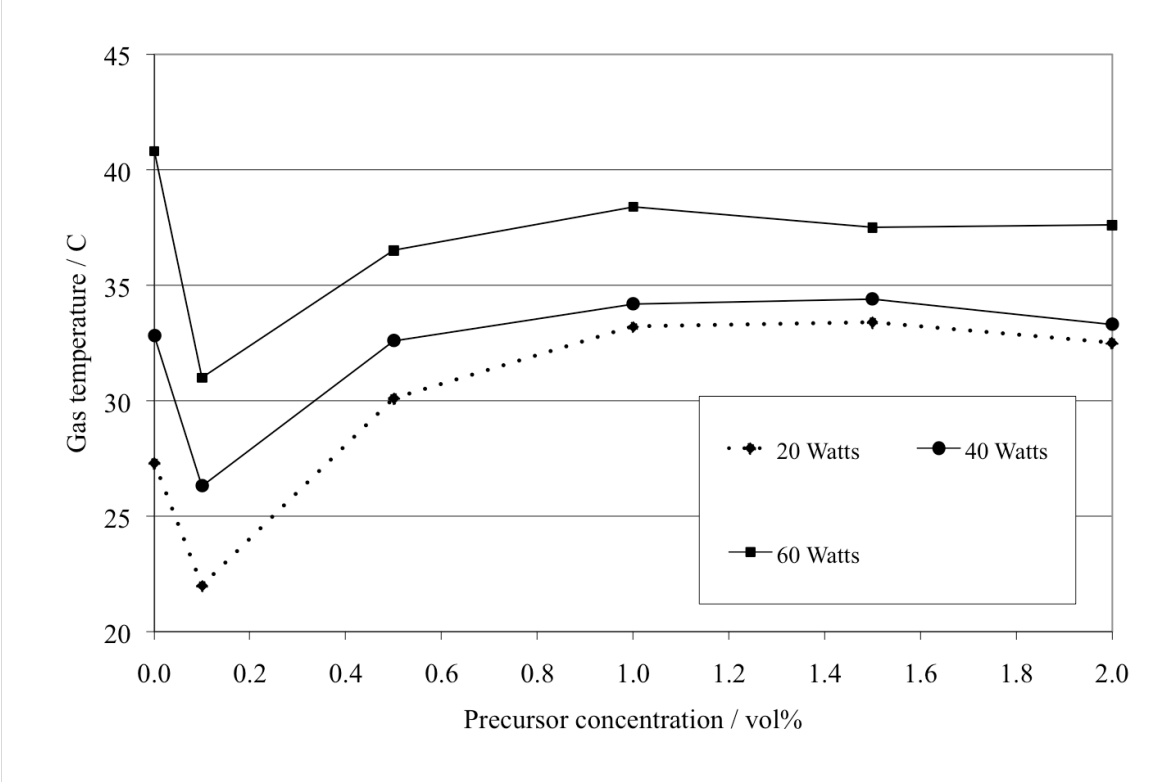

Figure 4.7 Effect of precursor on effluent temperature

Temperature observations allowed confirm non-equilibrium within the plasma equipping the system ready for nanofabrication.

4.4.Spectral analysis of reactive plasma components

Decomposition of acetylene and methane feedstock inside the argon plasma was scrutinized for presence of the reactive species. The emitted lines resulted mainly from the dissociative excitation of the CH_4/C_2H_2 molecules and from electron impact excitation of the radicals and atoms. One of the excitation path most commonly observed for CH_4 is

$$CH_4 + e \rightarrow CH^* + H_2 + H + e$$

Relative concentration of some of these species could be relatively estimated using the spectral data. Fig. 4.8 shows the decomposition of argon inside the capillary plasma reactor powered with 40 watts of applied power. This confirmed our ability to produce plasma using the capillary reactor and production of reactive species capable to ionize the feedstock.

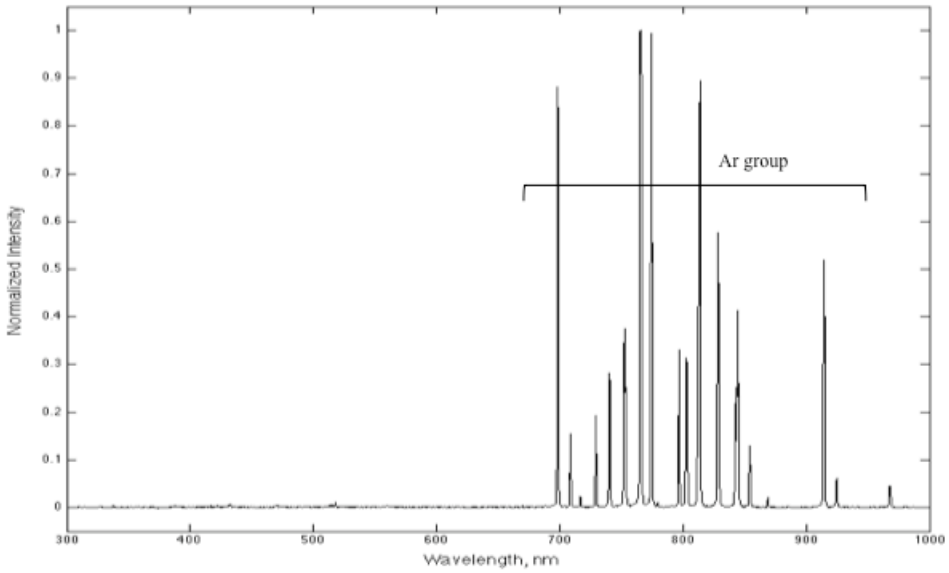

Figure 4.8 Argon emission spectrum

Emission species	Wavelength, nm	Normalized intensity
Ar	698.37	0.88
	765.67	1.00
	774.45	0.99

Table 1 Reactive species summary

Our ability to decompose acetylene and methane precursors was verified as well. Spectral data was attained for ionized argon/methane (Fig. 4.10) and argon/acetylene (Fig. 4.12) mixtures inside the capillary reactor in tube-ring powering configuration. Both spectrums demonstrated that the precursor gases were disassociated successfully and

yielded CH radicals needed for production of carbon-based material. Some peaks observed between the 450 and 500 nm point out to formation of hydrogen species within the gas discharge. It is thought that increasing their concentration can enable plasma to produce hydrogen ions that can play a role for treating the catalysts for carbon nanotube synthesis as well as for cleaning the plasma reactor during the deposition. Such data can also be used to estimate and tune deposition rates of the nanomaterials.

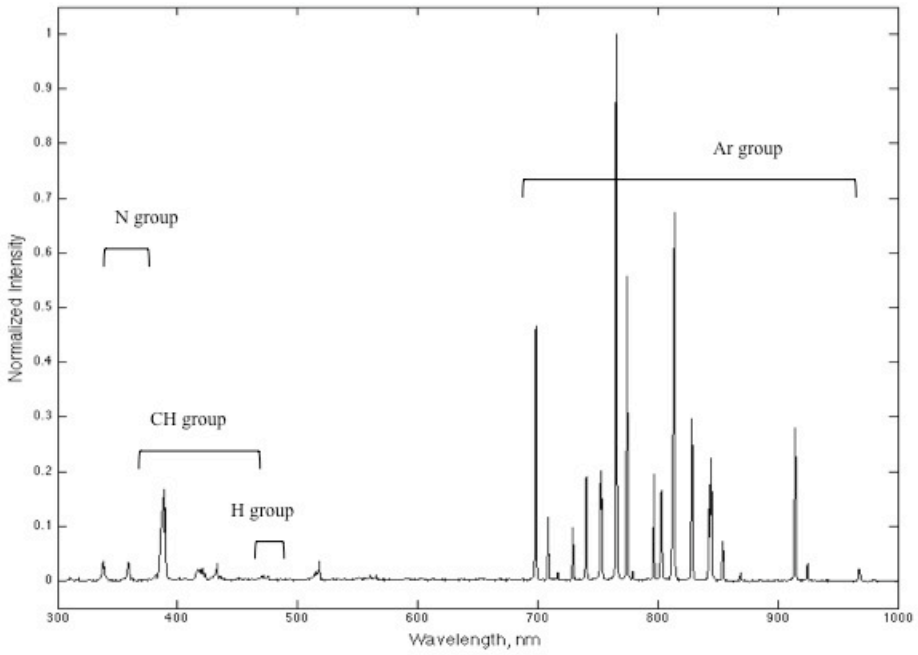

Figure 4.9 Argon/methane mixture emission spectrum

Emission species	Wavelength, nm	Normalized intensity
Ar	698.37	0.47
	765.67	1.00
	774.45	0.56
CH	387.64	0.14
	388.43	0.17
	389.74	0.13
N	359.15	0.03

Table 2 Reactive species summary

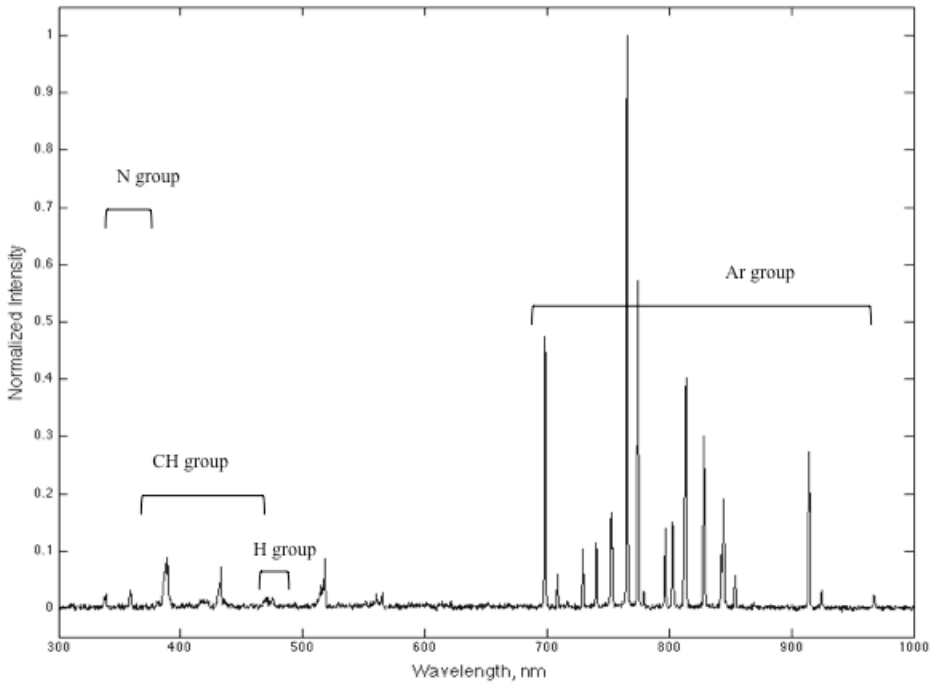

Figure 4.10 Argon/methane mixture emission spectrum

Emission species	Wavelength, nm	Normalized intensity
Ar	698.37	0.88
	765.67	1.00
	774.45	0.99
CH	388.43	0.09
	431.50	0.04
	432.81	0.07
N	359.15	0.03

Table 3 Reactive species summary

The mixtures used in this study were ionized with 30 Watts of applied power. The flow rate of argon used for data collection was 100 sccm producing a 1 vol% dilute mixture of methane or acetylene.

Presence of N ions was observed during the decomposition of the precursor however no N peaks are seen inside the argon plasma. Perhaps, addition of precursor opens up pathways for ionization of nitrogen that leaks into the reactors during processing.

The intensities of the peaks were found to vary linearly with the applied power, however no detailed study of the evolution behavior of the spectra with respect to power and gas flow has been carried out. All peaks were identified using NIST Atomic Spectra Database and publications available in plasma research [14], [15].

5. Fabrication and characterization of nanostructures

5.1. Introduction and sample preparation

In order to ignite plasma, electrode conditioning was found to be a necessary initial step. This preliminary preparation of the plasma reactor is thought to be viable for removing parasitic capacitance present at the electrode. The removal was carried out through application of electric power that exceeded the reactor's ignition power.

To ensure that the contamination was not hindering the deposition of materials, the substrates were wiped with acetone. Two types of samples were considered for experimentation with the microplasma treatment. For production of nanocrystaline metal oxides a bare silicon substrate was processed. A substrate covered with a thin layer of

oxide and Fe-Ni was used for production of carbon materials. To enhance the activation of the catalyst, the samples in the latter case were heated with the available hot plate prior to the deposition. To produce nanocrystaline metal oxide, the wire electrode of the capillary reactor in ring-wire configuration is cleaned with acetone prior to assembly.

During processing of the substrates, unwanted carbon deposition on the electrodes and in the reactor's inner walls was significant and dictated the number of times a reactor could be used before cleaning or replacement of components was required. No functional way to clean either of the plasma reactors was proposed other than using reactive hydrogen or oxygen species to remove reactor contaminants. Reactive hydrogen ions are known for their ability of etching amorphous carbon efficiently but no efficient parameters have been found under which adequate densities of hydrogen species could be generated from either methane or acetylene.

Contamination observed inside the linear plasma head during the feedstock decomposition was so significant that the plasma would extinguish in some cases within a few minutes of existence. Unwanted carbon deposition produced on the surface of the electrodes during the nanofabrication experiments is shown in Fig. 5.1.

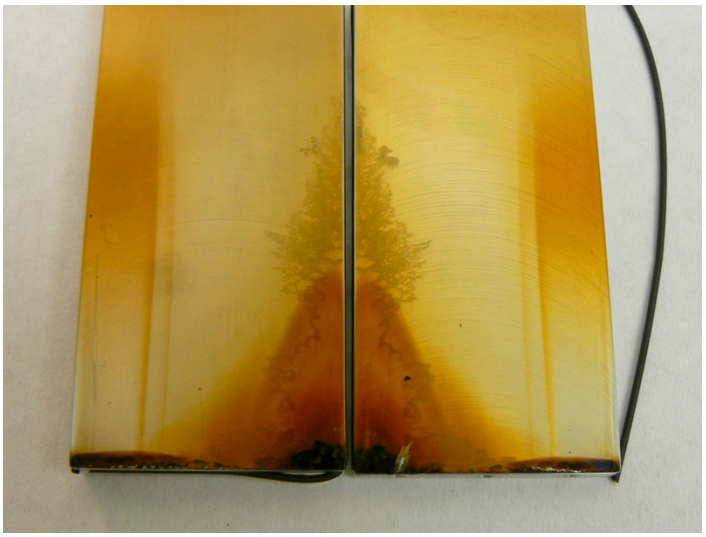

Figure 5.1 Contamination of linear plasma head electrodes

Capillary reactors would also become contaminated with use. However, using a new capillary reactor for processing each sample addressed this challenge and a set of new disposable reactors was manufactured each time prior to the deposition experiments.

5.2. Carbon nanoparticles

Despite of the observed contamination, Ni-Fe bearing substrates were treated with linear plasma head. The samples were heated to 350 °C. Only those flow ratios could be used for deposition that could maintain stable plasma. For methane, plasma glow can be obtained only at ratio smaller than 2.0 vol% in a mixture with helium. The constraints of the mass flow controllers enabled only small window of exploration, luckily it allowed for deposition of brown film with acetylene precursor.

A sample with was produced with this range in mind. A network of carbon structures with nanometer feature size was observed upon the microscopic investigation. Fig. 5.2 shows the size of the network and give the relative scale by which the width of

the single strand can be estimated. It is apparent that the produced strands are much narrower than the micrometer mark provided to describe the depositions scale.

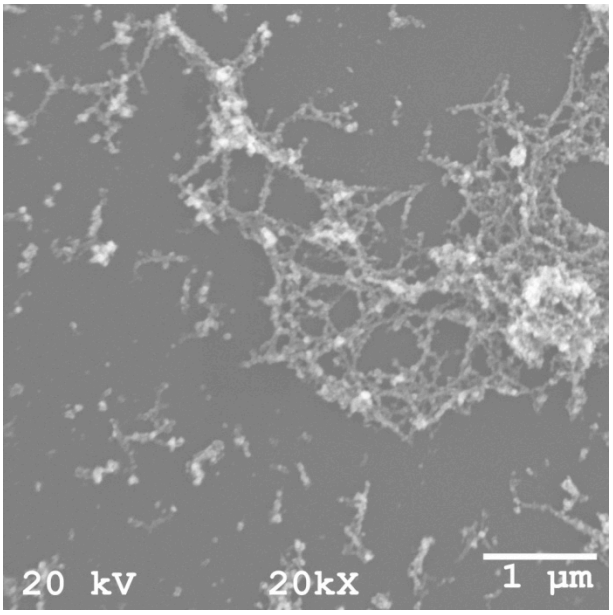

Figure 5.2 SEM analysis of carbon deposition produced with acetylene precursor

This sample was prepared using 1.0 vol % mixture of acetylene and helium in the linear plasma head at 30 watts of power.

TEM analysis (Fig. 5.3) of the material of this sample showed that it consisted of carbon nanoparticles of sizes smaller than 100 nm. Electron diffraction pattern showed that the material was crystalline.

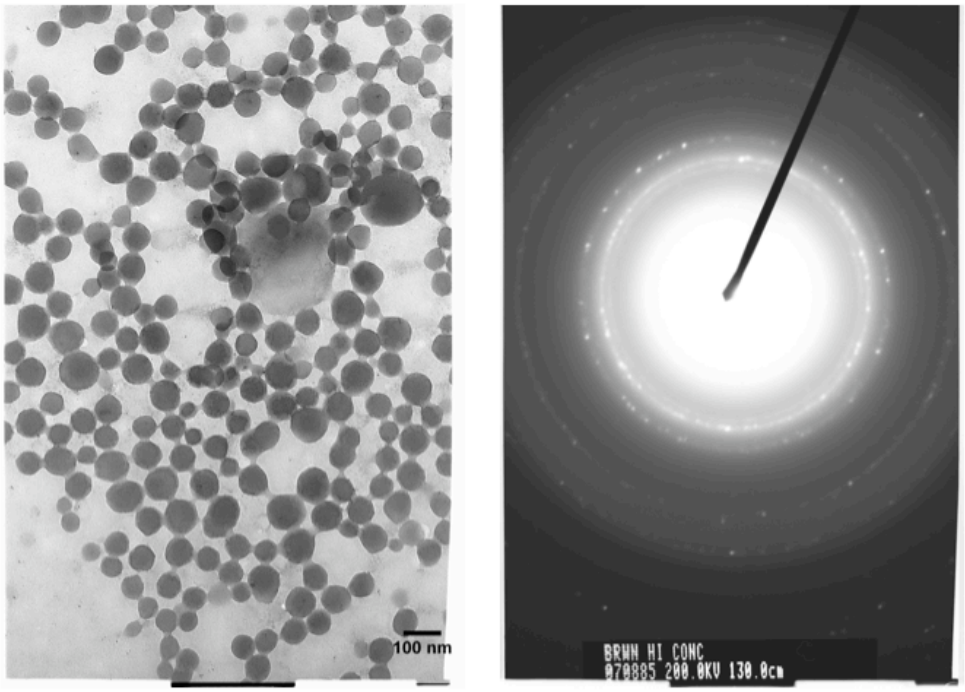

Figure 5.3 TEM analysis of deposition produced with acetylene precursor

5.3. Progress in carbon nanotube fabrication

With the aim of producing carbon nanotubes, deposition of carbon-based materials is also attempted using the capillary plasma reactor in tube-ring configuration. Samples in this case were also heated to 350 °C.

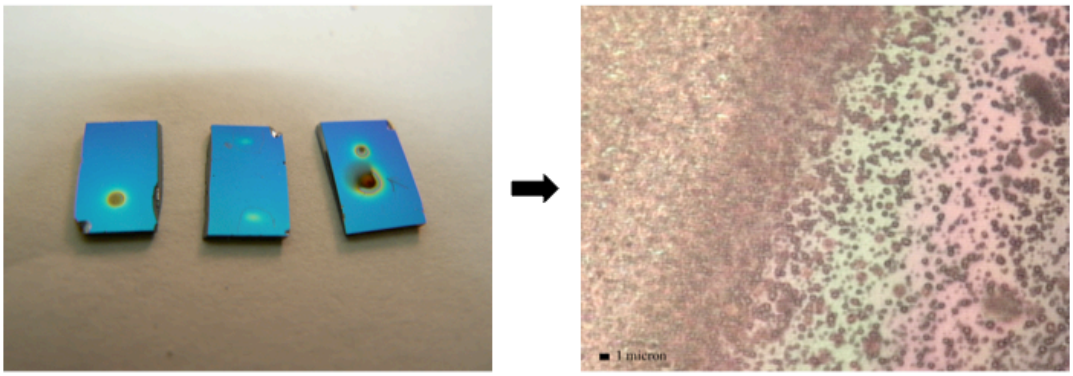

Figure 5.4 Carbon deposition on Ni-Fe substrate

Carbon deposition was obtained at the samples (Fig. 5.4) processed with plasma carrying methane and xylene precursors. In order to produce these samples a vapor of mixture of xylene solvent and ferrocene powder was added to the argon plasma. Both substrates shown in Fig 5.5 and 5.6 were processed for 1 minute and plasma at 30 watts. A 1.0 vol % mixture of methane and argon was used for the first case and 50-50 mixture of helium and helium carrying xylene vapor for the second case. Newly manufactured reactor was used for each run. The set up of the gas delivery system did not allow production of carbon material with argon when xylene precursor is employed.

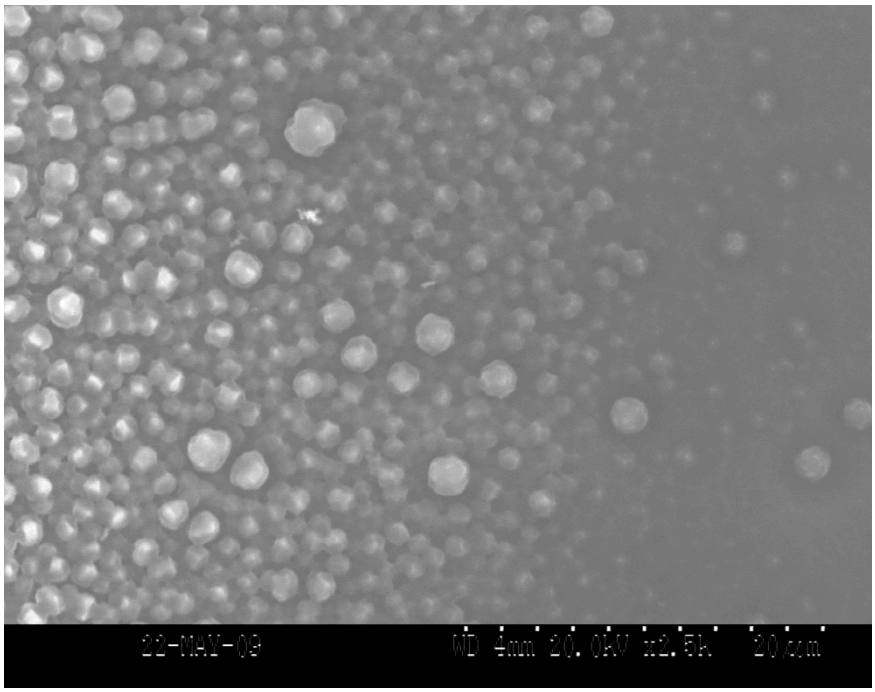

Figure 5.5 Carbon particle deposition produced with methane precursor

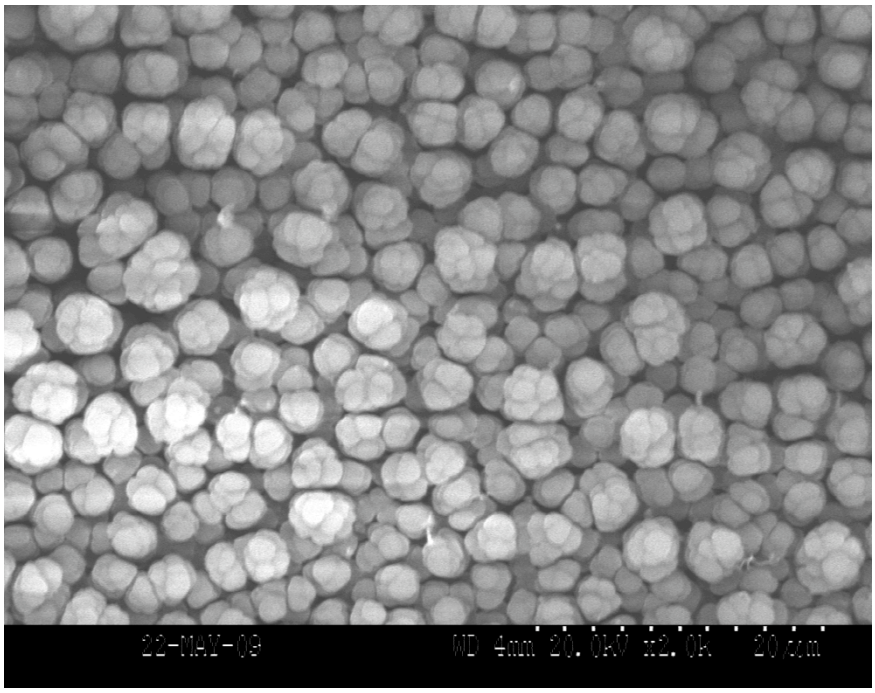

Figure 5.6 Carbon particle depostion produced with xylene precursor

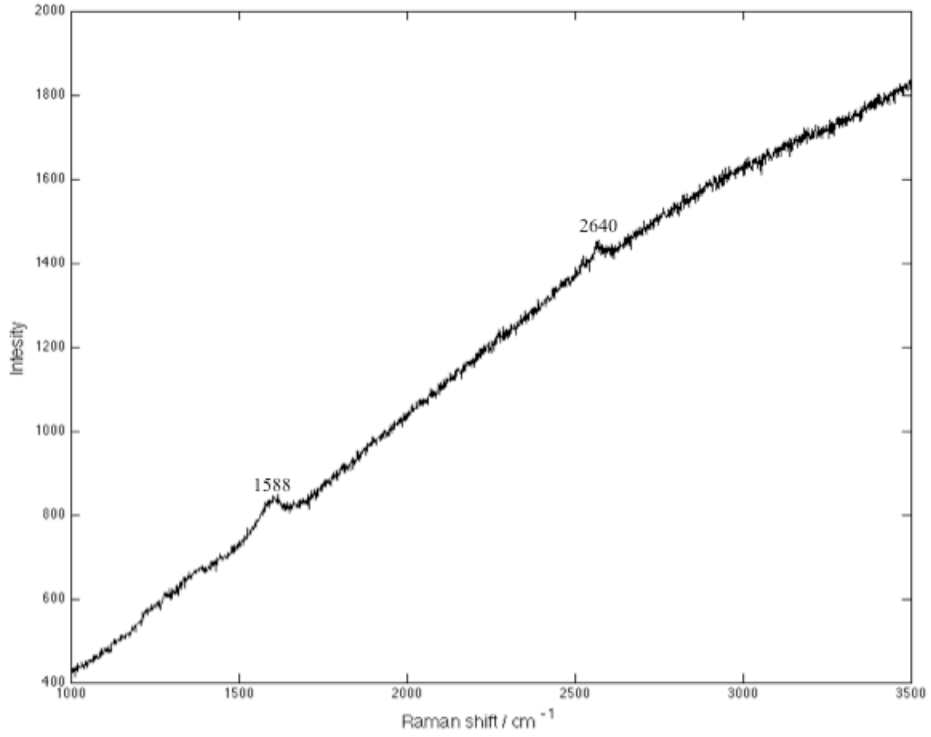

Figure 5.7 Raman spectroscopy of carbon particle

Energy shifts detected by Raman spectroscopy at the 1588 cm^{-1} and 2640 cm^{-1} peaks (Fig 5.7) describe the first of the samples containing crystalline carbon. Highly ordered graphite is known to exhibit 1582 cm^{-1} band and also show second order features in ranges of 2400 and 3300 cm^{-1}. The obtained results are correlated with the reported vibrational modes for graphitic materials found in literature [16].

Microscopic analysis of electrode's tip has shown a deposition of fibrous material (Fig. 5.8). Tubular shape of this material resembles a carbon nanotube however no TEM analysis was carried out to determine whether the produced structures were hollow.

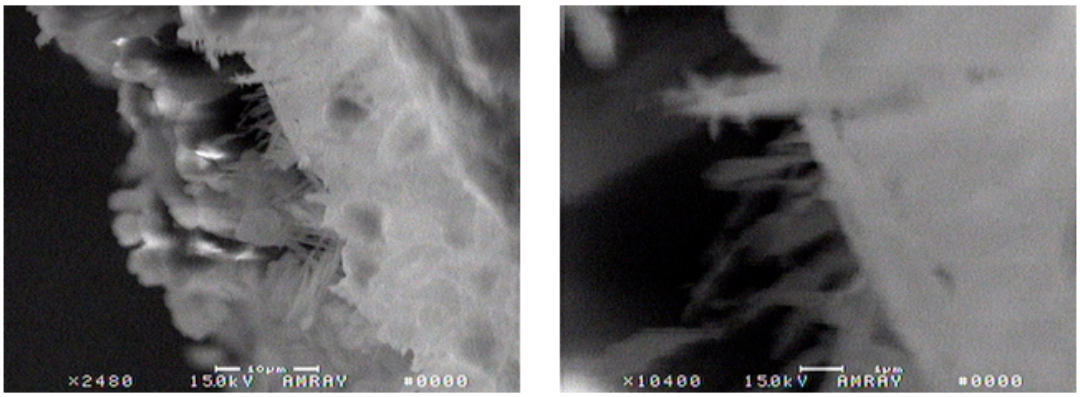

Figure 5.8 Carbon deposition at the electrode of the capillary reactor

Carbon nanotubes were not produced with certainty and further work is needed to explore fabrication parameter range.

5.4. Metal and metal oxide deposition

Deposition of metals was undertaken using a capillary reactor in ring-wire configuration. For this purpose three types of wire were used which included Ti, Ni and Mo. For each run the substrate was processed for 1 minute and was not heated. The reactors with three types of wire electrode yielded deposition (Fig. 5.9). It has been observed that when a thick wire of Ni (0.15 mm) was used as the reactor's electrode no film was deposited. However, when thinner wire was used 0.05 mm some deposition was attained (Fig. 5.10).

Argon was flown at 150 sccm for both cases and the power to initiate plasma was 30 Watts.

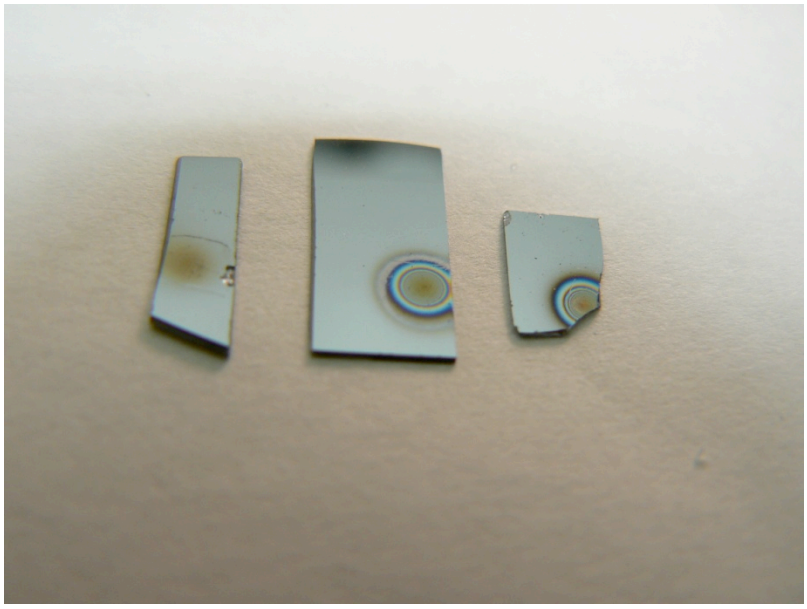

Figure 5.9 Metal deposition on Si substrate

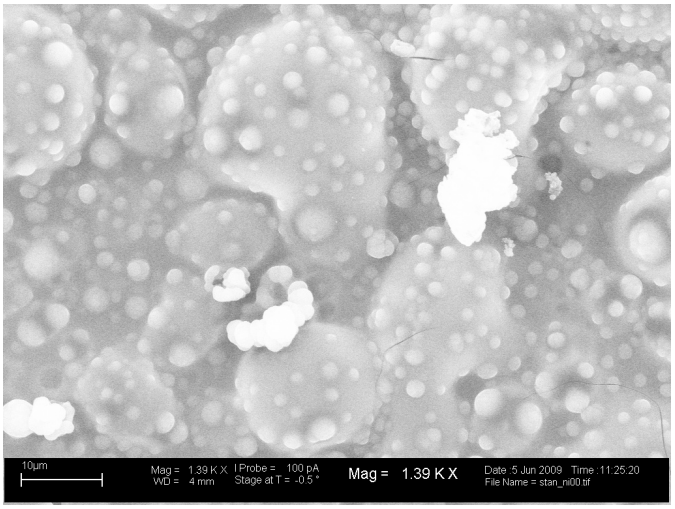

Figure 5.10 Deposited Ni film

Another metal deposition with the same gas and power parameters was attempted with molybdenum wire in place. Plasma did not ignite with this gas flow, however, decreasing it to 75 sccm yielded stable discharge. The gauge of the wire studied was 0.07 mm and this experiment has produced a film of structures (Fig. 5.10).

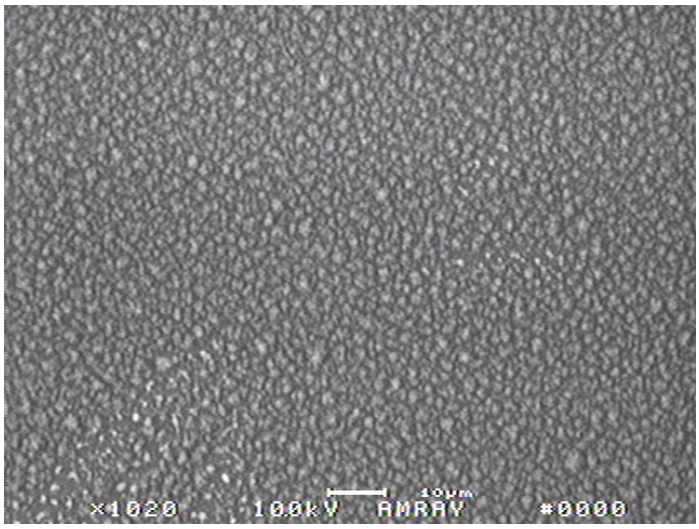

Figure 5.11 Deposited Mo film

Upon TEM analysis the film was found to consist of molybdenum nanorods shown in Fig. 5.12. According to the electron diffraction pattern, the produced material was crystalline MoO_3. The oxygen to produce this material was thought to come from the air surrounding the sample during processing. The average diameter of the nanorod is roughly estimated to fall below 20 nm.

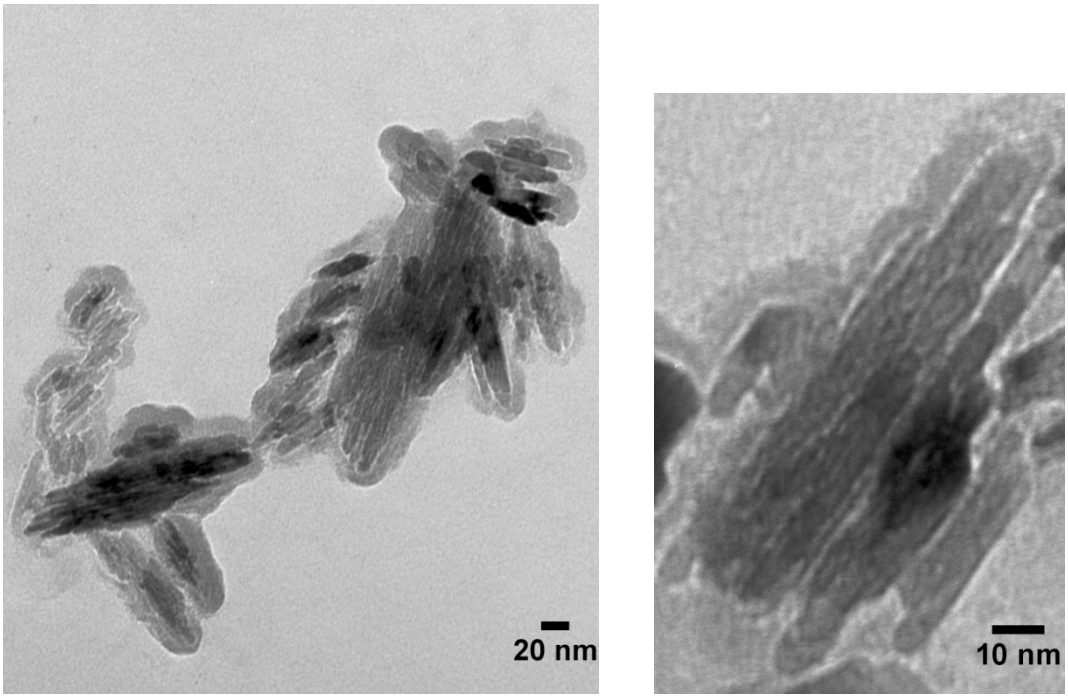

Figure 5.12 Molybdenum oxide nanorods

Since atmospheric microplasmas are highly reactive small portion of the electrode was consumed during processing, this also limited reactors use because the placement of the ring electrode had to be adjusted to maintain fixed electrode spacing.

5.5. Metal etching

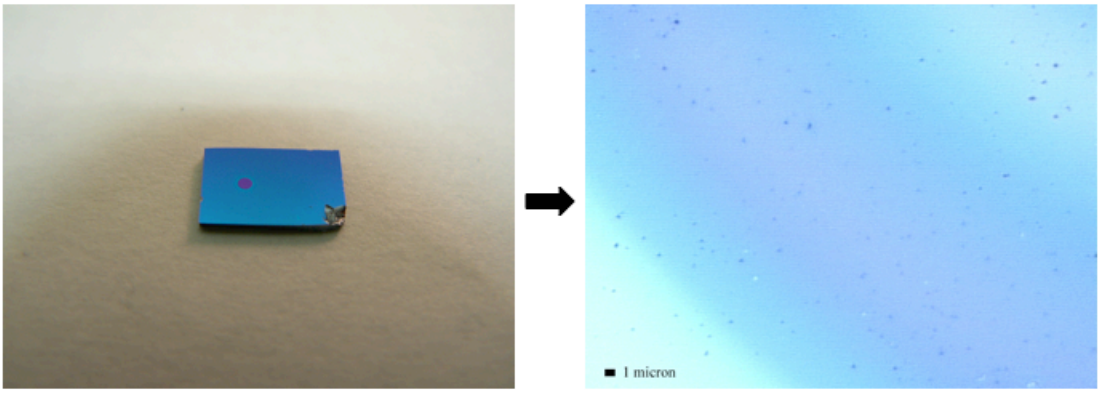

Figure 5.13 Etching of nickel film achieved using atmospheric microplasma

At high power argon microplasma was capable of etching the nickel-iron film deposited on a silicon substrate (Fig. 5.13). Upon microscopic analysis no thermal damage was observed leading to a speculation that the etching was completed through a non-thermal reactive mechanism. Also, as it was stated above in Section 4.2, the measured temperature of the ionized effluent was not sufficiently high to deteriorate nickel film thermally. To achieve etching, the nickel substrate was processed with argon plasma. Capillary reactor in tube-ring powering configuration was used to ionize argon flowing at rate of 100 sccm. Power applied to the reactor was 40 Watts and the sample was processed for 1 minute. Etching trials on similar nickel samples showed that

increasing the power and the gas flow supplied to the reactor gave an increase in the surface area etched away.

6. Conclusion

6.1. Summary

A setup that can accommodate different types of plasma reactors was put together. The analysis of the electrical characteristics of the plasma generated inside these reactors identified a unique regime of plasma operation. This regime, that we call microplasma, was investigated as a viable solution for producing nanostructrured and crystalline materials under atmospheric condition.

Using this setup, a number of advanced materials were deposited on silicon samples. Analysis with Raman spectroscopy and transmission electron microscopy found that the deposited carbon based materials were crystalline in nature. Molybdenum oxide deposited with this system was shown to feature structures of nanoscale dimensions.

6.2. Challenges and future work

During this study, various factors affecting the produced plasma discharges were observed. For a successful employment of microplasma in manufacturing, attention must be paid to design of the reactors. In particular, attention to electrode placement during the assembly of the capillary reactor must be paid. This practice can enable production of plasma characteristics invariable run-to-run. Precision in the electrode spacing can be assured, if investment into appropriate advanced micropositioning equipment is made.

Since the deposition of the metal oxide was found to relate to the electrode's geometry, an advanced study must be carried to determine this dependency. Experiments that consider different gauges of the electrode wire in the ring-wire configuration must be conducted. Once, the invariability in setup of the capillary reactors is established, a more detailed study of the carrier/precursor mixing ratios can be performed so the correlation between the plasma processes and the resulting deposition is more explicit.

In situ cleaning of the reactors must be worked out in order to conserve time and materials used up for manufacturing of new capillary reactors. To achieve this the system must be adapted for safe handling of hydrogen gas. The process of generating hydrogen ions from the hydrocarbon precursor can also be investigated. For continuation of the study without the in-situ cleaning, a process of making the capillary reactors with different powering configurations must be made more efficient.

Also possibility of using capillary reactors bundled in an array to increase processing area of a substrate must be explored. For this purpose, new powering and gas delivery schemes must be considered and efficiency of such setup investigated. If different gases are supplied to different rows of the array multiple processing steps can be carried out sequentially as the bundle is scanned over the target surface.

APPENDIX

Produced samples were analyzed using metrology equipment available at Semiconductor and Microsystems Fabrication Laboratory and NanoImaging Laboratory at Rochester Institute of Technology as well as facilities at University of Ulster. Some instruments used for sample analysis were scanning electron microscope (SEM), transmission electron microscope (TEM) and electron diffraction technique, Raman spectroscope, and an optical microscope.

The scanning electron microscope (SEM) is a type of electron microscope that images the sample surface by scanning it with a high-energy beam of electrons in a raster scan pattern. The electrons interact with the atoms that make up the sample producing signals that contain information about the sample's surface topography, composition and other properties such as electrical conductivity. For the investigation JEOL JSM-6400V SEM, Amray 1830 SEM, and LEO EVO50 SEM were used.

Transmission electron microscopy (TEM) is a microscopy technique whereby a beam of electrons is transmitted through an ultra thin specimen, interacting with the specimen as it passes through. An image is formed from the interaction of the electrons transmitted through the specimen; the image is magnified and focused onto an imaging device, such as a fluorescent screen, on a layer of photographic film, or to be detected by a sensor such as a CCD camera. In order to scrutinize samples JEOL JEM-100CXII tunnelling electron microscope was used electron diffraction patterning was also completed using this tool.

Raman spectroscopy is a spectroscopic technique used in condensed matter physics and chemistry to study vibrational, rotational, and other low-frequency modes in a system. It relies on inelastic scattering, or Raman scattering, of monochromatic light, usually from a laser in the visible, near infrared, or near ultraviolet range. The laser light interacts with phonons or other excitations in the system, resulting in the energy of the laser photons being shifted up or down. The shift in energy gives information about the phonon modes in the system.

References

1 M. Laroussi, T. Akan, "Arc-Free Atmospheric Pressure Cold Plasma Jets: A Review", Plasma Processes and Polymer, September 2007

2 National Research Council, National Research Council (U.S.), and Panel on Opportunities in Plasma Science and Technology, "Plasma Science: From Fundamental Research to Technological Applications", National Academies Press, January 1995

3 http://en.wikipedia.org/wiki/File:Ionization_energies.png

4 J. J. Shi, M. G. Kong, "Evolution of Discharge Structure in Capacitive Radio-Frequency Atmospheric Microplasmas", Physical Review Letters, March 2006

5 E. Stoffels, A. J. Flikweert, W. W. Stoffels, G. M. W. Kroesen, "Plasma needle: a non-destructive atmospheric plasma source for fine surface treatment of (bio)materials", Plasma Sources Science and Technology, August 2002

6 A. Schutze, J. Jeong, S. Babayan, J. Park, "The atmospheric-pressure plasma jet: a review and comparison toother plasma sources", IEEE transactions on plasma science, Vol. 26, No. 6, Decembet 1998

7 D. Mariotti, H. Lindstrom, A. C. Bose, K. K. Ostrikov, "Monoclinic beta-MoO3 nanosheets produced by atmospheric microplasma: application to lithium-ion batteries", Nanotechnology, October 2008

8 F. E. Osterloh, "Inorganic Materials as Catalysts for Photochemical Splitting of Water", Chemistry of Materials, December, 2007

9 Z. Pan, "Nanobelts of Semiconducting Oxides", Science, February 2001

10 P. Poizot, S. Laruelle, S. Grugeon, L. Dupont, J.M. Tarascon, "Nano-sized transition-metal oxides as negative-electrode materials for lithium-ion batteries", Nature, 2000 vol. 407 (6803) pp. 496-499

11 S. H. Lee, R. Deshpande, D. Benhammou, P. A. Parilla, A. H. Mahan, A. C. Dillon, "Metal oxide nanoparticles for advanced energy applications", Thin Solid Films, 2009 vol. 517 (12) pp. 3591-3595

12 S.J. Kim, T.H. Chung, S.H. Bae, "Characteristic study of atmospheric pressure microplasma jets with various operating conditions", Thin Solid Films, February 2009 vol. 517 (14) pp. 4251-4254

13 A. Pastol, Y. Catherine, "Optical emission spectroscopy for diagnostic and monitoring of CH plasmas used for a-C: H deposition", Journal of Applied Physics, 1990 vol. 23 (7) pp. 799-805

14 K. Clay, S. Speakman, G. Amaratunga, S. Silva, “Characterization of a‐C: H: N deposition from CH/N rf plasmas using optical emission spectroscopy”, Journal of Applied Physics, January 1996

15 R. Barni, A. Quintini, M. Piselli, C. Riccardi, “Experimental study of hydrogen plasma reforming by intermittent spark discharges”, Journal of Applied Physics, March 2008

16 Y. Wang, D. Alsmeyer, R. McCreery, "Raman spectroscopy of carbon materials: structural basis of observed spectra", Chemistry of Materials, April 1990